Thermochemical Properties, Pathway, and Kinetic Analysis on the Reactions of Benzene with OH: An Elementary Reaction Mechanism

Chiung-Chu Chen and Joseph W. Bozzelli*

Department of Chemical Engineering, Chemistry and Environmental Science, New Jersey Institute of Technology, Newark, New Jersey 07102

John T. Farrell

ExxonMobil Research and Engineering Company, Annandale, New Jersey 08801-3059

Received: November 26, 2003; In Final Form: February 27, 2004

Kinetics for the chemical activation reaction of the OH radical with benzene and unimolecular dissociation of the adduct are analyzed using quantum Rice−Ramsperger−Kassel (QRRK) theory for *k(E)* and master equation analysis for pressure falloff. Thermochemical properties and reaction path parameters are determined by ab initio and density functional calculations. Molecular structures and vibration frequencies are determined at the B3LYP/6-31G(d,p) and MP2(full)/6-31G(d) levels, with single point calculations for the energy at the B3LYP/6-311++G(2df,p)//B3LYP/6-31G(d,p), composite methods of CBS-Q, CBS-QB3 and G3(MP2) and the G3 methods. The OH addition to benzene forms a chemically activated prereactive complex with a shallow well (ca. 3 kcal mol^{-1}), which predominantly dissociates back to reactants. Additional reactions of the energized precomplex include stabilization, or forward reaction to form hydroxycyclohexadienyl radical, **C˙HDOH**, which has a well depth of 16 kcal mol^{-1}. This **C˙HDOH** adduct can either eliminate H atom to form phenol, undergo intramolecular addition of the radical to an unsaturated carbon site to form bicyclo[3.1.0]hexan-6-ol radical (**I** in Figure 2), or react back through the prereactive complex. The radical (**I**) can cleave a strained exocyclic, cyclopropane bond forming cyclopenta-2,4-dienylmethan-1-ol radical (**II** in Figure 2). Rate coefficients for reactions of the energized complex are obtained from canonical transition state theory. The high-pressure addition rate constant for OH + benzene → prereactive complex is calculated from variational transition state theory with a center-of-mass reaction coordinate approximation. A detailed mechanism with mass conservation and microscopic reversibility is assembled and used to identify the intermediates and products of the benzene + OH reaction for comparison with experiment. The prereactive complex has a small effect on the overall kinetics and can be considered negligible over the temperature and pressure range investigated. The most important product formation channel in the OH + benzene addition reaction system is formation of phenol plus H atom. Comparisons of our calculated rate constants with experimental data that exhibit complex temperature and pressure dependence of [OH] vs time shows very good agreement and illustrate that microscopic reversibility needs to be included in analysis of experimental data on this reaction system. The important products for benzene + OH addition are predicted to be **C˙HDOH** and phenol + H. At 800 K, product formation from cyclopentadiene intermediates is at least 3 orders of magnitude lower than phenol + H.

Introduction

Aromatic hydrocarbons constitute a significant fraction of transportation fuels and consequently a detailed understanding their oxidation chemistry is desirable. Modeling studies that couple elementary level kinetic mechanisms with multidimensional fluid dynamics are becoming computationally feasible and hold the promise of helping to ameliorate photochemical urban smog and optimize the performance of internal combustion engines. The detailed oxidation and pyrolysis kinetics of aromatics are less well understood than those for aliphatic hydrocarbons, however, reflecting in part the rich and intricate chemistry of the aromatic ring. Recent experimental and theoretical studies that have focused on understanding the reaction dynamics of prototypical systems have started to shed light on the key initial steps in aromatic fuel degradation.

The benzene + OH system has been the focus of numerous studies due to its relative simplicity and its practical and fundamental importance. As one example, the oxidative degradation of tropospheric benzene is initiated almost exclusively by OH. Since benzene and several of its degradation products are toxic and carcinogenic, it is important to understand the fate of atmospheric benzene. This requires a detailed kinetic model that is valid over temperatures of atmospheric relevance (250−400 K). Similarly, the auto ignition kinetics of aromatics at intermediate temperatures (∼700−1100 K) are strongly influenced by reactions with OH. Combustion strategies are presently under development that promise significant improve-

* Author for correspondence. E-mail: bozzelli@njit.edu. Telephone: (973) 596-5294. Fax: (973) 596-3586.

10.1021/jp0312823 CCC: $27.50
Published on Web 05/05/2004

ments in vehicle efficiency and emissions, and these strategies rely strongly on controlling the oxidation kinetics of the fuel. Additionally, the high temperature (>1200 K) oxidation and flame front consumption of aromatics initially involve reactions with the radicals H, OH, and O. These decomposition reactions include pathways that generate soot precursors and thus affect pollutant formation with aromatic fuels. Consequently, there is much interest in elucidating the important kinetic pathways for benzene + OH over a very wide temperature range.

Early experimental measurements of the rates for benzene + OH → products identified two main reaction channels, whose branching ratio depends strongly on temperature.[1−6] At low temperature, addition reactions predominate and the collisionally stabilized complex is the major intermediate formed (reaction 1). At temperatures near ∼325 K (depending on pressure), the decomposition of the complex becomes sufficiently fast to lead to a marked reduction in the bimolecular rate coefficient. As the temperature is raised further, the direct H abstraction channel increases in importance and is the dominant pathway under combustion conditions (reaction 2). The production of significant quantities of phenol in flow reactor and atmospheric chamber experiments has indicated the presence of an additional reaction channel.[7−10] This has been suggested to arise from H atom loss from the hydroxycyclohexadienyl complex through unimolecular elimination (reaction 3) and/or reaction with O_2.[11]

$$C_6H_6 + OH \rightarrow \mathbf{C^{\bullet}HDOH} \quad (1)$$

$$C_6H_6 + OH \rightarrow \text{phenyl} + H_2O \quad (2)$$

$$C_6H_6 + OH \rightarrow \text{phenol} + H \quad (3)$$

A number of theoretical studies have focused on characterizing the benzene + OH potential energy surface in order to explain the experimentally observed branching ratios, thermochemical properties, and rate coefficients.[12−16] Early studies that relied on semiempirical methods did not reproduce the experimental data well due to uncertainties in the energetics that were comparable to both the transition state barriers and relatively weak binding energy of the hydroxycyclohexadienyl adduct. Recently Berho et al.[14] estimated bond dissociation energies for a series of substituted cyclohexadienyl complexes using the B3LYP/6-31G(d) density functional for geometry optimization and BAC-MP4 single point calculations for energy parameters. Barckholtz et al.[15] carried out a mechanistic study of H, O, and OH reactions with several aromatics including benzene using potential energy surfaces calculated using the B3LYP density functional and rate coefficient estimation via nonvariational transition state theory with tunneling corrections. While the thermochemical enthalpies and barriers exhibit reasonable agreement with experiment, the kinetic rate coefficients are qualitatively incorrect. Tokmakov and Lin[16] recently presented a detailed analysis of reactions 1, 2, and 3 using several high level DFT and ab initio MO methods. They concluded that G3//B3LYP/6-311++G(d,p) theory is capable of accurately calculating thermochemical properties. They also calculated for the first time the properties of the benzene−OH hydrogen-bonded complex, and on the basis of their IRC analysis, they conclude that it is this complex, rather than the separated reactants, that is connected to the transition state for formation of hydroxycyclohexadienyl radical. Effective rate coefficients calculated using master equation, RRKM analysis, and a near 1−3 kcal mol^{-1} adjustment in the barrier demonstrated good agreement with selected experimental data on OH addition rates. They also indicate that the direct formation of phenol (reaction 3) is negligible over the temperature range 200−2500 K.

The present study is an extension of our earlier computational study[12] of the kinetics and thermochemistry of the benzene + OH system. Structures, intramolecular rotation barriers, and thermochemical properties are calculated using ab initio and density functional calculations. This study incorporates the results from our recent study of the hydroxycyclohexadienyl radical.[17] In addition to the three pathways represented by reactions 1−3, isomerization barriers and energetics are calculated for three higher energy pathways. The kinetics for the bimolecular reactions of the adducts are analyzed using quantum Rice−Ramsperger−Kassel (QRRK) theory for $k(E)$ with master equation and/or modified strong-collision analysis for pressure effects.

Methodology

All calculations are performed using the Gaussian 98 program suite.[18] The structural parameters are optimized at B3LYP/6-31g(d,p)[19] and MP2(full)/6-31g(d) levels of theory for the most stable conformer of each species. Harmonic vibration frequencies and zero-point vibrational energies (ZPVE) are computed at the same level. Transition state (TS) geometries are identified by the existence of only one imaginary frequency in the normal mode coordinate analysis, evaluation of the TS geometry, and the reaction coordinate's vibrational motion. The B3LYP/6-31g-(d,p), B3LYP/6-311++g (2df,p)// B3LYP/6-31g(d,p), and composite methods of CBS-Q,[20,21] CBS-QB3 [22] and G3(MP2)[23] with both MP2(full)/6-31g(d) and B3LYP/6-31g(d,p) determined geometries, are utilized to calculate total energies in this study. The CBS-Q and G3(MP2) calculations with B3LYP/6-31g(d,p) and MP2(full)/6-31g(d) geometries are referred to as CBSQ//B3LYP, CBSQ//MP2, G3MP2//B3LYP, and G3MP2//MP2 in this study. The initial addition reaction 1, the most important product formation reaction 3, and the H-abstraction reaction 2 are also studied at a higher calculation level, the G3 theory level of Curtiss et al.[24]

Thermodynamic Properties: $\Delta H_f^\circ{}_{298}$, $S^\circ{}_{298}$, and $C_p(300)$ to $C_p(1500)$. The scheme below shows isodesmic reactions IR1−IR10 that are used to determine $\Delta H_f^\circ{}_{298}$ for intermediate radicals and products. Calculations are performed on each species in the reaction to determine $\Delta H_{rxn,\ 298}$. $\Delta H_f^\circ{}_{298}$ values of the target species in a reaction are determined from the $\Delta H_{rxn,298}$ and evaluated literature $\Delta H_f^\circ{}_{298}$ values of the remaining species. Enthalpies of formation for transition states are calculated using an average calculated energy difference between the reactants and products, where these are each determined on an absolute basis using the work reactions as described in our previous study.[25] Our thermochemical and kinetic parameters are incorporated into a small elementary reaction mechanism, which is numerically integrated for comparison of our model with a range of experimental data at varied temperature, pressure, and reaction times.

Entropies ($S^\circ{}_{298}$) and heat capacities ($C_p(T)$'s, 300 ≤ T/K ≤ 1500) are calculated using the rigid-rotor-harmonic-oscillator approximation. Contributions from hindered rotors to $S^\circ{}_{298}$ and $C_p(T)$ are determined by direct integration over energy levels. Energy levels are calculated from solution of the Schroedinger equation using free rotor wave functions with potentials representing the intramolecular rotation potential energy curves[26,27] on the reactants, intermediates, transition states and products. Use of this internal rotation partition function accounts for contributions to entropy from the rotational conformers of each rotor. The number of optical isomers and spin degeneracy of unpaired electrons were also incorporated for calculation of $S^\circ{}_{298}$ and $C_p(T)$.

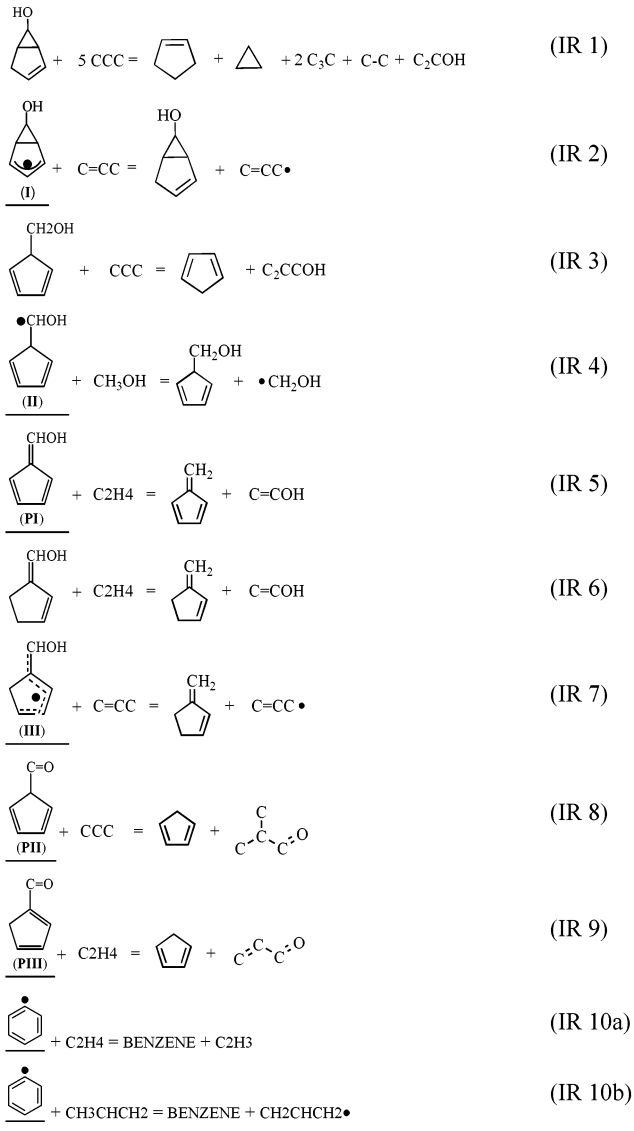

Kinetic Analysis. High-pressure limit rate constants are determined from the following: vibration partition functions from all frequencies (torsions omitted), external rotation partition functions from the determined molecular structures, internal rotor partition functions from the detailed analysis of each internal rotor. These data are converted into macroscopic kinetic parameters using established statistical mechanics procedures.

The chemically activated and stabilized **C•HDOH** adducts have access to a number of reaction paths, which can vary with both pressure and temperature. It is important to include the pressure effects in the determination (estimation) of the kinetic parameters and branching ratios to stabilization and new product channels, as well as dissociation back to reactants. Kinetic parameters are derived for product formation from the chemically activated adduct resulting from bimolecular association and from unimolecular, thermal dissociation of the stabilized adduct. These parameters are estimated using a multifrequency quantum Rice−Ramsperger−Kassel (QRRK) analysis for $k(E)$ with the steady-state assumption on the energized adduct, a Boltzmann thermal distribution of the adduct when formed, and master equation analysis for falloff.

The current version of the QRRK computer code utilizes a total of $3n - 6$ frequencies expressed as a reduced set of three frequencies (low−medium−high, sum of three sets equals $3n - 6$) that accurately reproduce the molecule's (adduct's) heat capacity ($C_p(T)$'s).[28−30] Molecular density-of-state functions are constructed through direct convolution of single frequency density functions on a 10 cm^{-1} grid. The functions corresponding to each reduced frequency set are explicitly convolved into a relative density-of-states ($\rho(E)$), which is normalized by the partition function (Q). The inclusion of one external rotation, corresponding to the symmetric top, is incorporated into the calculations by convolving the vibration density function with the proper rotational density function. A detailed description of this and comparisons of the $\rho(E)/Q$ ratios with the direct count $\rho(E)/Q$ ratios are shown to be in good agreement.[30] The program provides a chemical activation analysis on complex reaction system with a large number of adducts (wells) and product sets. The resulting kinetic parameters have been incorporated into small detailed mechanisms that have reproduced and extended experimental data in many complex reaction systems[25,31−34] as well as in this study. The QRRK formalism used in this work is described by Chang et al.[31] $(\Delta E)^\circ_{down}$ of 600 and 1000 (cal mol^{-1})[35,36] are used in master equation analysis for He and Ar as third body, respectively. An energy interval of 0.08 kcal mol^{-1} is used in the master equation analysis for chemically activation.

The ChemRate program[37] was also used to calculate the high-pressure limit rate constants and rate constants of reactions 1 and 3. $(\Delta E)^\circ_{down}$ of the bath gas and the energy interval for solving master equation are the same values used in the QRRK analysis.

Detailed Reaction Mechanism and Chemkin Analysis. A moderately small elementary reaction mechanism is developed from the chemical activation and unimolecular dissociation reaction analysis along with radical generation and intermediate association reactions where these are important. This mechanism is implemented in the Chemkin suite of mechanism integration codes[38] and is utilized to analyze and understand the kinetic processes as a function of time, temperature, and pressure and to compare the model against experimental results in the literature. The mechanism includes microscopic reversibility for all the elementary reactions with reverse rate constants determined from the forward rate constant, the thermodynamic parameters, and microscopic reversibility.

Results and Discussion

1. Geometries and Vibrational Frequencies. The geometries of all species are optimized at the B3LYP/6-31G(d,p) level. The intermediates (**I**, **II**, and **III**) and transition states (**TS1**, **TS2**, **TS3, TS4** and **TS5**) are also optimized at MP2(full)/6-31G(d) levels (shown in italics in Table 1). We were unable to locate transition states **TS6**, **TS7**, **TS8**, and **TS9** in calculations at the MP2(full)/6-31G(d) level, however. The geometries of all species optimized at B3LYP/6-31G(d,p) and MP2/6-31G(d) levels are available in the Supporting Information. Differences of DFT and MP2 bond lengths are within 0.02 and 0.12 Å for intermediates and transition states, respectively. Bond angles and dihedral angles are within 3.7° between B3LYP/6-31g(d) and MP2/6-31G(d) geometries, with the exception of dihedral angles of **TS4** (12.2°). The vibration frequencies and moments of inertia for all species are also listed in Table 1. The torsion frequencies corresponding to the hindered rotors are shown in Table 1 (bold).

2. $\Delta H_f^\circ_{298}$. The vibrational frequency contributions to ZPVE are scaled by 0.9806, 0.9661, and 0.8929 for B3LYP/6-31g-(d,p), MP2(full)/6-31G(d), and HF/6-31g(d) theoretical frequencies,[39] respectively. The frequencies are not scaled in calcula-

TABLE 1: Vibration Frequencies and Moments of Inertia for Model Stable (Parent) Molecules and Model Free Radicals

prereactive complex	frequencies (cm^{-1})[a]
PRI	17*i*, 71, 135, 140, 410, 417, 493, 618, 619, 694, 716, 861, 873, 976, 978, 1009, 1013, 1019, 1060, 1066, 1181, 1200, 1202, 1352, 1380, 1516, 1521, 1635, 1643, 3180, 3190,
460.9, 792.6, 969.2[b]	3197, 3208, 3209, 3229, 3736
PRII	121*i*, 86*i*, 25, 37, 96, 412, 414, 621, 621, 703, 716, 873, 874, 984, 985, 1017, 1017, 1020, 1065, 1066, 1181, 1203, 1204, 1352, 1381, 1522, 1522, 1648, 1649, 3181,
239.6, 478.8, 644.9	3190, 3190, 3205, 3205, 3214, 3699
236.7, 472.6, 636.4	*57, 62, 116, 142, 163, 400, 408, 561, 622, 641, 698, 858, 859, 915, 916, 1027, 1029, 1073, 1084, 1090, 1212, 1232, 1389, 1393, 1465, 1539, 1541, 1670, 1824, 3225, 3234, 3247, 3248, 3256, 3273, 3761*

complex	frequencies (cm^{-1})
I	228, **270**, 314, 376, 434, 543, 651, 674, 741, 800, 825, 869, 915, 932, 963, 1030, 1036, 1064, 1079, 1093, 1150, 1175, 1261, 1283, 1297, 1343, 1413, 1421, 1484, 3111, 3173,
272.4, 799.6, 952.1	3183, 3206, 3227, 3238, 3788
270.2, 789.4, 939.5	*235*, **283**, *331, 388, 442, 559, 682, 707, 756, 823, 856, 917, 944, 972, 997, 1056, 1071, 1099, 1106, 1144, 1183, 1207, 1296, 1316, 1332, 1348, 1431, 1464, 1550, 3178, 3235, 3247, 3267, 3287, 3298, 3743*
II	109, **115**, 273, 359, **447**, 550, 626, 666, 723, 740, 804, 846, 885, 952, 965, 982, 1010, 1018, 1117, 1123, 1175, 1203, 1243, 1315, 1341, 1405, 1435, 1568, 1655, 3019, 3189,
357.5, 797.6, 880.1	3205, 3216, 3236, 3242, 3757
364.7, 766.5, 835.6	*116*, **134**, *286, 365*, **454**, *551, 639, 713, 739, 770, 818, 861, 903, 910, 936, 1014, 1046, 1054, 1139, 1147, 1204, 1247, 1281, 1339, 1375, 1437, 1467, 1577, 1645, 3099, 3253, 3254, 3263, 3280, 3286, 3711*
III	149, 198, 252, **352**, 446, 490, 533, 645, 664, 738, 811, 821, 848, 926, 949, 964, 1052, 1115, 1145, 1151, 1201, 1268, 1328, 1341, 1387, 1409, 1466, 1524, 1620, 2992, 3014,
255.6, 951.9, 1196.3	3209, 3219, 3229, 3242, 3806
PI	145, 208, 278, 490, **537**, 587, 646, 695, 719, 768, 828, 899, 917, 926, 948, 1027, 1108, 1117, 1190, 1223, 1316, 1374, 1385, 1446, 1523, 1611, 1710, 3204, 3208, 3221, 3232,
242.8, 920.4, 1163.2	3246, 3784
PII	**81,** 110, 340, 444, 518, 573, 737, 750, 819, 836, 943, 958, 961, 971, 1022, 1034, 1043, 1122, 1131, 1193, 1257, 1320, 1409, 1416, 1549, 1646, 1816, 2926, 3096, 3213,
267.9, 893.9, 1053.1	3224, 3244, 3249
PIII	131, 196, **272**, 376, 498, 527, 710, 726, 825, 886, 894, 928, 966, 968, 1025, 1031, 1121, 1132, 1222, 1261, 1360, 1405, 1412, 1429, 1563, 1652, 1768, 2896, 3044, 3071,
242.1, 924.4, 1155.5	3211, 3222, 3242

transition states	frequencies (cm^{-1})[a]
TS1	328*i*, 112, 132, **217**, 391, 408, 609, 611, 664, 726, 800, 839, 898, 968, 971, 992, 1009, 1025, 1045, 1060, 1177, 1186, 1199, 1342, 1377, 1498, 1510, 1599, 1621, 3182, 3191,
429.2, 710.4, 924.5	3201, 3211, 3212, 3230, 3749
423, 671.9, 876.5	678*i*, *144, 146*, **252**, *419, 451, 637, 639, 702, 792, 866, 942, 985, 1007, 1040, 1055, 1064, 1114, 1124, 1133, 1175, 1242, 1258, 1295, 1418, 1564, 1591, 1732, 1749, 3244, 3253, 3264, 3272, 3275, 3288, 3721*
TS2	1251*i*, 70, 110, **164**, 350, 411, 447, 611, 634, 686, 728, 789, 834, 914, 968, 993, 997, 1007, 1037, 1077, 1106, 1185, 1189, 1323, 1338, 1343, 1477, 1512, 1620, 1638, 3177,
324.5, 1049.8, 1365.5	3185, 3197, 3203, 3208, 3758
313.2, 1001.7, 1303.5	*2316i*, 84, *123*, **183**, *367, 487, 518, 655, 691, 721, 819, 882, 1020, 1022, 1070, 1078, 1112, 1120, 1132, 1133, 1172, 1219, 1270, 1278, 1378, 1533, 1616, 1646, 1940, 1966, 3238, 3248, 3262, 3268, 3268, 3737*
TS3	979*i*, 210, **294**, 366, 421, 484, 502, 531, 624, 647, 685, 771, 812, 830, 898, 959, 983, 1003, 1041, 1100, 1179, 1190, 1192, 1280, 1353, 1374, 1503, 1522, 1608, 1638, 3173,
336.8, 708.2, 1017.4	3186, 3193, 3210, 3219
323.9, 695.4, 999.7	*1541i, 215*, **291**, *385, 456, 519, 554, 611, 649, 728, 756, 828, 873, 901, 983, 1031, 1045, 1053, 1101, 1161, 1174, 1229, 1241, 1299, 1322, 1409, 1565, 1589, 1703, 1746, 3235, 3247, 3255, 3272, 3278, 3764*
TS4	698*i*, 225, **307**, 340, 398, 476, 516, 593, 636, 697, 732, 799, 841, 907, 976, 1023,
298.7, 762.8, 974.7	1030, 1091, 1129, 1142, 1156, 1207, 1284, 1302, 1320, 1410, 1432, 1487, 1570, 2995,
292.8, 746.9, 948.4	3176, 3187, 3192, 3202, 3217, 3802
	1159i, *239*, **310**, *344, 425, 495, 530, 648, 719, 798, 799, 876, 939, 987, 1047, 1062, 1096, 1153, 1177, 1189, 1208, 1247, 1319, 1349, 1354, 1424, 1515, 1536, 1970, 3089, 3241, 3245, 3251, 3261, 3287, 3751*
TS5	478*i*, 170, 205, **341**, 405, 417, 542, 572, 699, 722, 803, 820, 837, 943, 952, 979, 1039, 1056, 1102, 1113, 1145, 1215, 1247, 1284, 1312, 1384, 1425, 1444, 1565, 3083, 3205,
278.2, 856.2, 1005.6	3214, 3228, 3240, 3254, 3802
292.8, 746.9, 948.4	*582i*, *201*, *230*, **353**, *427, 438, 570, 705, 712, 751, 841, 849, 880, 961, 1002, 1035, 1107, 1128, 1146, 1167, 1243, 1310, 1360, 1409, 1426, 1443, 1533, 1541, 1580, 3297, 3360, 3382, 3398, 3409, 3429, 4102*
TS6	1255*i*, *51*, 201, 235, **345**, 449, 526, 590, 649, 704, 724, 773, 848, 881, 921, 937, 1080, 1093, 1096, 1152, 1169, 1204, 1290, 1332, 1341, 1453, 1474, 1503, 1536, 1983, 3211,
249.2, 964.6, 1200	3227, 3231, 3239, 3255,3808
TS7	754*i*, 142, 201, 251, 280, 447, 485, **520**, 582, 634, 703, 724, 763, 825, 884, 908, 914, 935, 1028, 1108, 1118, 1183, 1216, 1313, 1363, 1379, 1439, 1525, 1620, 1648, 3211,
263.3, 931.9, 1156.8	3218, 3223, 3236, 3249, 3789
TS8	1205*i*, **53,** 93, 154, 236, 420, 540, 567, 674, 709, 721, 787, 815, 865, 947, 953, 962, 997, 1023, 1043, 1119, 1132, 1192, 1261,1321, 1399, 1418, 1573, 1653, 1666, 2962,
324.8, 848.6, 1003	2975, 3212, 3223, 3243, 3254
TS9	932*i*, 141, 184, 210, **271**, 369, 453, 518, 532, 709, 743, 822, 889, 926, 929, 970, 971, 992, 1029, 1128, 1132, 1200, 1277, 1318, 1395, 1422, 1428, 1532, 1624, 1657, 2954,
255.2, 959, 1192.6	3027, 3055, 3219, 3239, 3247

[a] B3LYP/6-31G(d,p) and MP2(full)/6-31G(d) theoretical frequencies. Frequencies and moments of inertia optimized at MP2(full)/6-31G(d) levels are shown in italics. The torsion frequencies corresponding to the hindered rotors are shown in boldface. [b] Moments of inertia in amu $Bohr^2$.

TABLE 2: Total Energy (at 298 K) Differences between TS's and Reactants, Intermediates, and Products[a] (in kcal/mol)

			//B3LYP/6-31G(d,p)			//MP2(full)/6-31g(d)				
reaction		G3	G3MP2	CBS-Q	CBS-QB3	G3MP2	CBS-Q	CBS-QB3	B3LYP[b]	B3LYP_B[c]
1	benzene + OH ⇒ **TS1**	0.86	3.64	−2.95	−2.37	6.31	−1.50	−0.96	6.31	−1.50
	C•HDOH ⇒ TS1	18.62	19.19	17.91	18.12	20.02	17.11	17.32	20.02	17.11
2	benzene + OH ⇒ **TS2**	5.97	6.52	1.55	1.61	12.51	7.60	7.80	12.51	7.60
	phenyl + H_2O ⇒ **TS2**	9.40	9.10	5.91	6.09	10.80	7.26	7.47	10.80	7.26
3	**C•HDOH ⇒ TS3**	26.29	27.16	13.13	13.00	27.39	12.03	12.14	25.49	24.44
	phenol + H ⇒ **TS3**	7.30	11.34	−2.72	−2.60	13.48	−1.28	−1.00	6.01	5.88
4	**C•HDOH ⇒ TS4**		34.82	35.09	35.28	37.60	38.33	38.41	38.04	37.74
	I ⇒ TS4		15.86	15.38	15.63	19.09	19.75	19.89	16.75	14.65
5	**I ⇒ TS5**		12.56	11.63	11.74	13.79	13.64	13.73	11.41	9.85
	II ⇒ TS5		10.78	7.31	7.48	12.62	10.51	11.35	7.92	7.93
6	**II ⇒ TS6**		19.92	19.45					18.20	17.15
	III ⇒ TS6		38.51	44.16					42.37	40.99
7	**II ⇒ TS7**		29.25	27.21					29.11	27.42
	PI + H ⇒ **TS7**		4.83	4.06					3.11	3.14
8	**II ⇒ TS8**		36.56	36.13					34.01	33.88
	PII + H ⇒ **TS8**		12.52	10.63					7.41	7.85
9	**III ⇒ TS9**		48.28	52.23					45.46	45.76
	PIII + H ⇒ **TS9**		11.50	9.04					3.84	4.58

[a] Reaction enthalpies include thermal correction and zero-point energy correction. [b] On the basis of 6-31G(d,p) basis set. [c] B3LYP/6-311++G(2df,p)//B3LYP/6-31G(d,p).

TABLE 3: Isodesmic Reaction Enthalpies (in kcal mol^{-1})

				//B3LYP/6-31G(d,p)			//MP2(full)/6-31g(d)						limited
reaction	G3	CBSQ	CBS-QB3	G3MP2	CBS-Q	CBS-QB3	G3MP2	CBS-Q	CBS-QB3	B3LYP[a]	B3LYP_B[b]	SD[c]	errors[d]
IR 1				−1.67	−1.17	−1.18	−1.82	−1.23	−1.24	1.26	0.13	±0.46	±1.8
IR 2				4.61	5.59	5.50	4.36	5.49	5.41	5.52	4.95	±0.21	±2.62
IR 3				−1.28	−0.17	−0.18	−1.34	−0.11	−0.12	−0.75	−0.79	±0.23	±1.25
IR 4				1.42	1.41	1.37	1.27	1.97	2.65	2.81	1.84	±0.26	±2.3
IR 5				1.97	4.41					2.76	2.50	±0.61	±1.07
IR 6				−1.55	1.03					−2.28	−2.34	±0.91	±1.07
IR 7				7.66	9.23					9.28	9.07	±0.45	±1.89
IR 8				−0.42	0.98					0.46	−0.05	±0.35	±1.42
IR 9				2.97	5.47					3.49	3.54	±0.63	±1.4
IR 10a	4.26	4.47	4.18									±0.11	±1.22
IR 10b	27.67	28.20	27.54									±0.25	±0.94

[a] On the basis of the 6-31G(d,p) basis set. [b] B3LYP/6-311++G(2df,p)//B3LYP/6-31G(d,p). [c] Statistical standard deviations. [d] Uncertainty in enthalpy values for the reference compounds.

TABLE 4: Enthalpies (at 298 K) of Intermediates and Products Calculated from the Isodesmic Reactions (IR1−IR10)[c]

				//B3LYP/6-31G(d,p)			//MP2(full)/6-31g(d)				
$\Delta H°_{f,298}$	G3	CBS-Q	CBS-QB3	G3MP2	CBS-Q	CBS-QB3	G3MP2	CBS-Q	CBS-QB3	B3LYP[a]	B3LYP_B[b]
phenyl radical	83.01	83.38	82.90								
I				29.89	28.90	28.99	30.14	29.00	29.08	28.97	29.54
II				35.60	35.61	35.65	35.75	35.05	34.37	34.21	35.18
III				15.37	11.23					14.48	14.75
PI				9.49	7.05					8.70	8.96
PII				7.07	5.67					6.19	6.70
PIII				−2.38	−4.88					−2.90	−2.95
TS1	29.32			31.00	27.06	27.46	32.74	27.38	27.76	25.80	25.46
TS2	34.72			34.85	30.76	30.88	38.69	34.59	34.79	27.12	29.22
TS3	36.53			38.98	24.94	24.93	40.17	25.10	25.30	35.48	34.89
TS4				45.20	45.10	45.31	48.21	48.90	49.01	47.26	46.06
TS5				44.01	41.80	41.95	45.54	44.41	44.88	42.00	41.23
TS6				53.54	56.12					54.60	53.39
TS7				60.77	61.52					55.54	56.06
TS8				71.44	70.28					67.61	67.77
TS9				64.89	63.49					63.96	63.13

[a] On the basis of 6-31G(d,p) basis set. [b] B3LYP/6-311++G(2df,p)//B3LYP/6-31G(d,p). [c] Literature data used in isodesmic reaction to determine $\Delta H°_{f,298}$ of species studied in this work: $\Delta H°_{f,298}$ of (C_2H_4) = 12.54 ± 0.1;[59] (CC) = −20.04 ± 0.07;[60] (C_3C) = −32.25 ± 0.28;[60,61] (C═CC) = 4.879;[62] (CCC) = −25.02 ± 0.12;[60] (C═COH) = −29.59 ± 0.47;[63] (C═CC═O) = −20.06;[64] (C_2CC═O) = −51.57 ± 0.37;[65] (C_2COH) = −65.07 ± 0.22;[66] (C_2CCOH) = −67.80 ± 0.2;[67] (YCCC) = 12.74 ± 0.14;[68] (YPE) = 8.5 ± 0.21;[69] (YPD) = 33.2 ± 0.93;[70] (CDYPE) = 27.6;[71] (fulvene) = 53.6.[70] Bond dissociation energy (kcal mol^{-1}) $\Delta H°_{f,298}$ of (C═CC−H) = 88.12;[71] (H−CH_2OH) = 98.17.[71]

tions of the vibration component of the thermal contribution to enthalpy. Total energy differences (at 298 K) between TS and reactants, intermediates, and products determined at different theory levels are listed in Table 2. Isodesmic reaction enthalpies (IR1−IR10) calculated at the different computation levels are listed in Table 3. $\Delta H_f°_{298}$ of reactant, intermediate radicals, and products from group balance isodesmic reactions at various calculation levels are listed in Table 4.

Enthalpy values from each calculation level are listed in Table 4. Our data show that the G3MP2 values result in higher $\Delta H_f°_{298}$ values than CBSQ calculations on corresponding structures. They further show that geometries optimized with the MP2

TABLE 5: Ideal Gas Phase Thermodynamic Properties[a]

species		$H_f°_{298}$[b]	$S°_{298}$[c]	$C_p(300)$[c]	$C_p(400)$	$C_p(500)$	$C_p(600)$	$C_p(800)$	$C_p(1000)$	$C_p(1500)$
H		52.1	27.36	4.97	4.97	4.97	4.97	4.97	4.97	4.97
O		59.55	38.47	5.23	5.14	5.08	5.04	5.01	5.01	4.98
OH		8.96	43.88	7.15	7.1	7.07	7.06	7.13	7.33	7.87
H_2O		−57.8	43.72	8.17	8.88	9.56	10.2	11.3	12.1	12.98
C_6H_6		19.81 ± 0.12	64.37	19.92	27.09	33.25	38.38	45.87	51.05	58.31
PHOH		−23.03 ± 0.14	75.43	24.9	32.45	38.64	43.54	50.62	55.49	
phenyl		83.1 ± 1.70	68.81	18.94	25.47	31	35.44	41.9	46.34	52.85
PRII	TVR[d]	26.13	86.49	28.93	35.83	41.78	46.68	54.04	59.32	67.5
C•HDOH[17]		10.39 ± 1.55	79.24	27.17	35.46	41.91	46.87	54.05	59.14	67.02
I	TVR[d]		75.94	24.30	32.61	39.50	44.92	52.69	58.04	66.07
	internal rotor[e]		3.69	2.08	1.80	1.58	1.43	1.26	1.17	1.07
	total	29.33 ± 3.21	79.63	26.38	34.41	41.08	46.35	53.95	59.21	67.14
II	TVR		77.13	23.32	31.11	37.68	42.93	50.59	55.93	64.01
	internal rotor		9.11	5.52	5.63	5.41	5.09	4.45	3.92	3.06
	total	35.34 ± 3.00	86.24	28.84	36.74	43.09	48.02	55.04	59.85	67.07
III	TVR		79.03	25.31	33.00	39.51	44.76	52.46	57.85	65.99
	internal rotor		2.69	2.30	2.30	2.23	2.12	1.87	1.67	1.36
	total	13.30 ± 2.78	81.72	27.61	35.30	41.74	46.88	54.33	59.52	67.35
PI	TVR		76.35	23.56	30.69	36.73	41.59	48.69	53.63	61.04
	internal rotor		1.17	2.28	2.78	2.96	2.98	2.81	2.55	1.99
	total	8.27 ± 2.12	77.52	25.84	33.47	39.69	44.57	51.50	56.18	63.03
PII	TVR		73.40	22.14	29.54	35.85	40.94	48.42	53.60	61.25
	internal rotor		4.68	3.52	3.55	3.18	2.76	2.12	1.75	1.34
	total	6.37 ± 2.21	78.08	25.66	33.09	39.03	43.70	50.54	55.35	62.59
PIII	TVR		75.80	22.49	29.56	35.72	40.77	48.30	53.55	61.27
	internal rotor		3.95	2.55	2.67	2.63	2.56	2.42	2.33	2.09
	total	−3.63 ± 2.47	79.75	25.04	32.23	38.35	43.33	50.72	55.88	63.36
TS1	TVR		78.99	24.07	31.64	38.03	43.15	50.67	55.94	63.98
	internal rotor		2.97	2.79	2.60	2.27	1.99	1.61	1.40	1.18
	total	28.12 ± 2.00	81.96	26.86	34.24	40.30	45.14	52.28	57.34	65.16
TS2	TVR		81.6	25.3	33	39.48	44.66	52.16	57.3	64.92
	internal rotor		3.77	1.94	1.74	1.57	1.44	1.28	1.18	1.08
	total	33.52 ± 3.02	85.37	27.24	34.74	41.05	46.10	53.44	58.48	66.00
TS3	TVR		77.79	24.94	32.90	39.46	44.65	52.15	57.29	64.90
	internal rotor		3.34	1.99	1.94	1.82	1.69	1.49	1.36	1.18
	total	35.33 ± 3.34	81.13	26.93	34.84	41.28	46.34	53.64	58.65	66.08
TS4	TVR		77.25	23.96	31.73	38.21	43.39	50.93	56.20	64.17
	internal rotor		2.69	2.51	2.66	2.50	2.24	1.80	1.52	1.22
	total	46.96 ± 5.27	79.94	26.47	34.39	40.71	45.63	52.73	57.72	65.39
TS5	TVR		78.71	24.21	31.94	38.42	43.57	51.03	56.23	64.13
	internal rotor		3.80	1.96	1.96	1.96	1.94	1.84	1.70	1.43
	total	43.76 ± 7.02	82.51	26.17	33.90	40.38	45.51	52.87	57.93	65.56
TS6	TVR		83.64	24.86	32.37	38.77	43.93	51.50	56.74	64.56
	internal rotor		3.29	2.06	2.21	2.29	2.28	2.14	1.95	1.57
	total	54.83 ± 6.51	86.93	26.92	34.58	41.06	46.21	53.64	58.69	66.13
TS7	TVR		80.51	26.83	34.32	40.53	45.47	52.64	57.59	65.01
	internal rotor		2.53	2.06	2.45	2.65	2.71	2.61	2.39	1.88
	total	64.19 ± 6.92	83.04	28.89	36.77	43.18	48.18	55.25	59.98	66.89
TS8	TVR		80.40	25.52	33.28	39.76	44.94	52.49	57.69	65.31
	internal rotor		4.95	3.61	3.53	3.13	2.70	2.08	1.72	1.31
	total	70.86 ± 6.31	85.35	29.13	36.81	42.89	47.64	54.57	59.41	66.62
TS9	TVR		80.09	25.65	33.10	39.48	44.65	52.27	57.54	65.26
	internal rotor		3.95	2.55	2.67	2.63	2.56	2.42	2.33	2.09
	total	61.15 ± 5.69	84.04	28.20	35.77	42.11	47.21	54.69	59.87	67.35

[a] Thermodynamic properties are referred to a standard state of an ideal gas gas and pure enantiometer of the most stable conformer at 1 atm. [b] In kcal mol^{-1}. [c] In cal mol^{-1} K^{-1}. [d] The sum of contributions from translation, external rotation, vibration, optical isomer, and spin degeneracy. [e] $S°_{298}$ and Cp(T) contributions from hindered rotors.

calculation method result in higher $\Delta H_f°_{298}$'s than values resulting from the same level of calculation using the B3LYP geometry. The differences between use of MP2 vs B3LYP geometry in the G3MP2 calculations are less than 1.0 and 3.8 kcal mol^{-1} for intermediates and transition states, respectively. CBSQ has larger differences between MP2 and B3LYP geometries, 1.7 and 4.7 kcal mol^{-1}, for the respective intermediates and transition states. The largest deviations are between the G3MP2//MP2 and CBSQ//B3LYP results. The G3 calculation results in a value between the G3MP2 and CBSQ. We recommend $\Delta H_f°_{298}$ of **TS1**, **TS2**, and **TS3** from the G3 calculation values, each with a downward adjustment of 1.2 kcal mol^{-1} in the barrier as discussed below. Similar adjustments have been made in previous calculation analysis on this benzene + OH system.[16] Recommended $\Delta H_f°_{298}$ for intermediates **I** and **II** and transition states **TS4** and **TS5** are from an average of the following four calculation methods: G3MP2//MP2, G3MP2//B3LYP, CBSQ//MP2, and CBSQ//B3LYP. All other transition states (**TS6**, **TS7**, **TS8**, and **TS9**), products (**PI**, **PII**, and **PIII**), and intermediate **III** are from an average of the G3MP2//B3LYP and CBSQ/B3LYP.

The accuracy of our theoretical $\Delta H_f°_{298}$ values is assected by several factors: the choice of the working chemical reactions used to cancel calculation errors, the calculation level (method

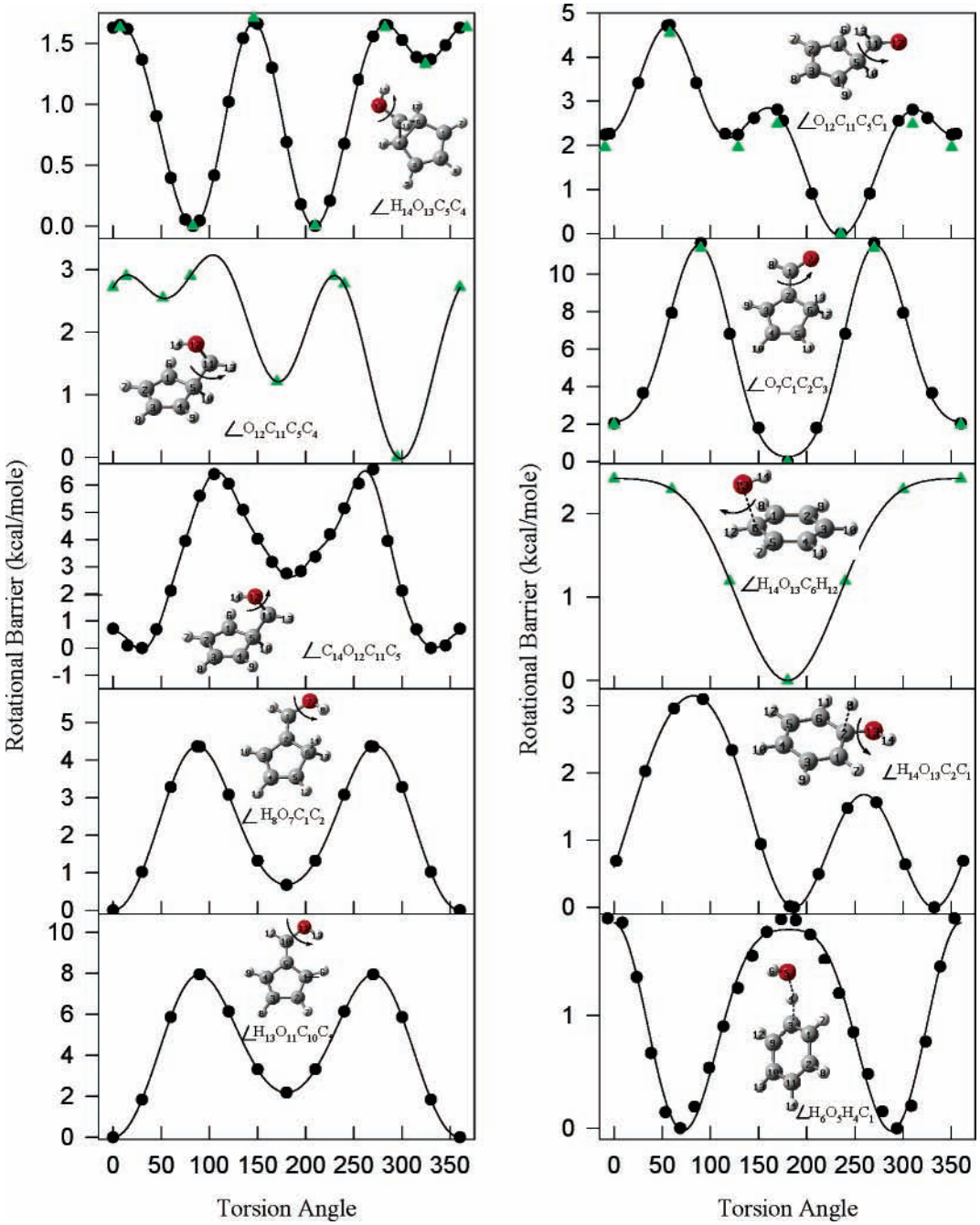

Figure 1. Potential barriers of internal rotations. Points are calculated values at B3LYP/6-31G(d,p) level of theory. Lines are results of Fourier expansion equation, F1. The total energies where the zero point vibrational energy (ZPVE) and the thermal correction to 298 K (HT_{298}) are included are shown as triangles.

+ basis set) applied to calculate the electronic energy, the uncertainty in ZPVE and thermal corrections, and the accuracy for $\Delta H_f^\circ{}_{298}$ of reference compounds. We assumed that our calculations on species in the isodesmic reactions have similar error ranges for ZPVE and thermal corrections; we assign the cumulative uncertainty corrections to be 0.44 kcal mol^{-1} from Scott and Radom.[39] The errors of $\Delta H_f^\circ{}_{298}$ were calculated by summing the deviations between various levels, the errors from the ZPVE and thermal corrections, and the maximum uncertainties in enthalpy of the reference compounds. The maximum uncertainly in enthalpy values for the reference compounds and the statistical standard deviations from calculation levels in the isodesmic reactions are listed in Table 3. The errors of $\Delta H_f^\circ{}_{298}$ for the intermediates, transition states and products are listed in Table 5.

3. Rotational Barriers

Potential barriers for internal rotations of **I**, **II**, **III**, **PI**, **PII**, **PIII**, and **TS3** are calculated at the B3LYP/6-31G(d,p) level. The internal barrier of **TS2** is calculated using molecular mechanics force field (MMFF), and the barrier of **TS1** is calculated at G3MP2//B3LYP/6-31g(d) to provide higher accuracy values in entropy and heat capacity contribution from the hindered internal rotor. The potential energy as a function of the dihedral angle is determined by varying the torsion angle in 30° intervals and allowing the other parameters to be optimized; the minima and maxima on the torsional potential are then fully optimized. One exception is the calculation on **TS2** where bond lengths of the forming O−H bond and the cleaving H−C bond were fixed at the length of most stable

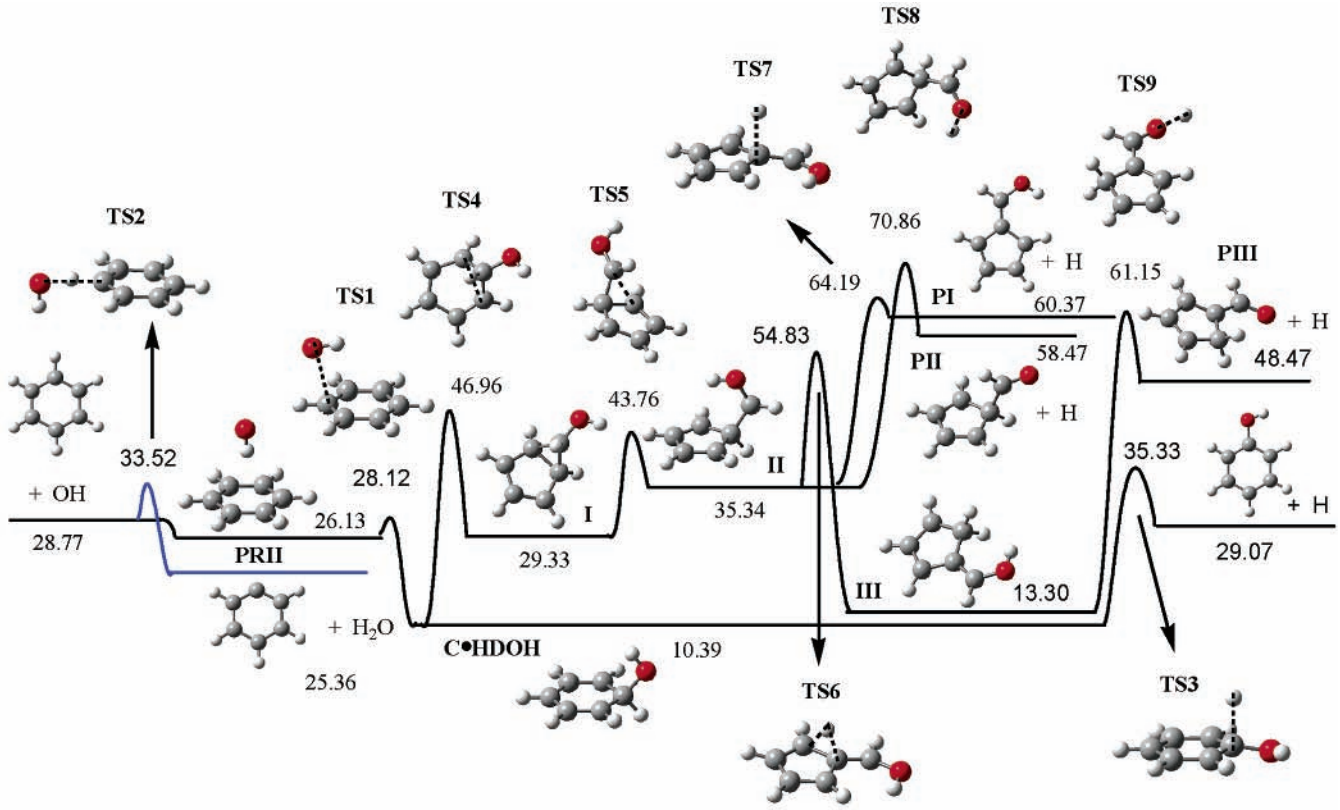

Figure 2. Potential energy diagram for the chemical activation reaction calculations on OH addition to benzene and for dissociation reactions of the stabilized adduct, along with abstraction of phenyl H atoms by OH (via **TS2**) which forms phenyl radical + H_2O. Numbers are $\Delta H_f°_{298}$ (kcal mol^{-1}) used in this study for kinetics analysis (listed in Table 5).

conformer. The O−H−C angle was also fixed at that of the most stable conformer. The barriers for internal rotations are calculated from the differences between the total energy of each conformation and that of the most stable conformer. The calculated rotation barriers vs torsion angle are shown in Figure 1. A Fourier series was used to represent the potential calculated at discrete torsion angles (shown as lines in Figure 1)

$$V(\Phi) = a_0 + a_i \cos(i\Phi) + b_i \sin(i\Phi), \quad i = 1, 2, 3, \ldots \quad \text{(F1)}$$

where values of the coefficients are calculated to provide the true minima and maxima of the torsional potentials with allowance of a shift of the theoretical extrema of angular positions. Further description on this method to calculate S and $C_p(T)$ contributions from the internal rotors are reported by Lay et al.[26]

4. $S°_{298}$, and C_p(300) to C_p(1500). $S°_{298}$ and $C_p(T)$'s were calculated using the rigid-rotor-harmonic-oscillator approximation based on scaled vibrational frequencies, molecular mass, and moments of inertia from the optimized B3LYP/6-31G(d,p) structures (prereactive complex **PRII** is based on MP2(full)/6-31G(d) structure). The ROTATOR program calculates the $S°(T)$'s and $C_p(T)$'s from hindered rotor contributions by direct integration over energy levels resulting from solution of the Schroedinger equation for the corresponding internal rotor using calculated intramolecular rotation potential energy curves.[26,27] The analysis includes contributions of the conformers transcended by each internal rotor and includes hindered rotor contributions to S and Cp at all temperatures.

$S°_{298}$ and $C_p(T)$'s for species in the benzene + OH system are summarized in Table 5. TVR represents the sum of contributions from translations, external rotations, and vibrations for $S°_{298}$ and $C_p(T)$'s. The symbol IR represents the $S°_{298}$ and $C_p(T)$ contributions from hindered rotors. The thermodynamic parameters: $\Delta H_f°_{298}$, $S°_{298}$, and C_p(300) to C_p(1500) used in kinetics analysis for this OH addition to benzene reaction system are listed in Table 5. We note that values are only accurate to 1 digit after the decimal for the kcal mol^{-1} units. Values are listed for each rotor, and coefficients for equation F1 are listed in the Supporting Information.

5. Benzene + OH Reaction System. Figure 2 shows the potential energy diagram used for the chemical activation calculations of OH addition to benzene and for dissociation reactions of the stabilized adduct. The abstraction of H atoms by OH (via **TS2**) which forms phenyl radical + H_2O, is also illustrated in Figure 2. The values of $\Delta H_f°_{298}$ for the intermediates, transition states and products are listed in Table 5.

OH addition to benzene forms a chemically activated prereactive complex which has a very shallow well (ca. 3 kcal mol^{-1}) and predominantly dissociates back to reactants under all conditions. Additional reactions of the energized precomplex include stabilization (formation of the resonance stabilized hydroxycylcohexadienyl radical, **C•HDOH** (adduct)) which has a near 16 kcal mol^{-1} well depth. This **C•HDOH** adduct can either eliminate H atom to form phenol, undergo intramolecular addition of the carbon radical site to an unsaturated carbon forming the bicycle[3.1.0]hexan-6-ol radical **I**, or react back to the prereactive complex. The radical **I** can cleave a strained exocyclic cyclopropane bond to form cyclopenta-2,4-dienylmethan-1-ol radical (**II**). Intermediate **II** can undergo H atom elimination via two channels to form an olefin (**PI**) or an aldehyde (**PII**), or it can react through a lower barrier (**TS6**) via a 1,2 H atom shift in concert with a corresponding diene shift. This forms a stabilized cyclopentylidenemethan-1-ol radical (**III**) where this diene is conjugated with the radical on the methyl group and the conjugation extends through the radical

site to the oxygen**.** This radical (**III**) will β-scission the hydroxyl hydrogen resulting in cyclopenta-1,3-dienecarbaldehyde (**PIII**) + H, where the diene is conjugated with the carbonyl group.

An asymmetric Eckart calculation for H tunneling as described in Yamada et al.,[40] Schwartz et al.,[41] Louis et al.[42] and Knyazev et al.[43] is used to calculate the tunneling factor ($\Gamma(T)$) for H-abstraction (**TS2**), H shift (**TS6**), and H elimination (**TS3**, **TS7**, **TS8** and **TS9**). The imaginary frequencies of **TS2** (1263 cm^{-1}), **TS3** (391 cm^{-1}), **TS6** (648 cm^{-1}), **TS7** (376 cm^{-1}), **TS8** (743 cm^{-1}), and **TS9** (557 cm^{-1}) used in Eckart tunneling calculation are adjusted (down) from the HF/6-31g(d) determined imaginary frequency of 3157, 977, 1619, 940, 1858, and 1392 as recommended by Schwartz et al. The values of Γs at 300, 800, and 1500 K are

Temperature (K)	TS2	TS3	TS6	TS7	TS8	TS9
300	58.3	54.2	1.55	11.1	5190	6680
800	1.93	2.03	1.06	1.65	2.20	2.20
1500	1.23	1.24	1.02	1.12	1.23	1.23

This tunneling influence on H-elimination through **TS7**, **TS8**, and **TS9** are ca. 1.4, 5.1, and 5.2 kcal mol^{-1} in barrier at 300 K and 0.3, 0.6, and 0.6 kcal mol^{-1} at 1500 K, respectively. The effect is not significant when considering the reaction barriers of 60−70 kcal mol^{-1}. The tunneling effects are more important in H-abstraction via **TS2** (to phenyl + H_2O) and H-elimination through **TS3** (to final products phenol + H atom) since these reaction barriers are much lower.

5a. Initial Reaction: OH Addition to Benzene to form C•HDOH. In our recent study of the hydroxycyclohexadienyl radical (**C•HDOH**),[17] the $\Delta H_f°_{298}$ calculated for this species was 10.39 kcal mol^{-1}.

$$\text{benzene} + \text{OH} \xleftrightarrow{\text{TS1}} \textbf{C•HDOH} \qquad (1)$$

The low-temperature (240−340 K) experimental activation barriers for this OH addition reported by Lorenz et al.[3] (0.994 kcal mol^{-1}), Baulch et al.[44] (0.676 kcal mol[1]), and Tully et al.[2] (0.537 kcal mol^{-1}) are in good agreement with the G3 calculated energy barrier of 0.86 kcal mol^{-1} (enthalpy differences between **TS1** and reactants at 298 K). Lin et al.[45] and Knispel et al.[5] reported negative barriers of 2.82 and 0.696 kcal mol^{-1}, respectively, at temperatures between 298 and 385 K. Our ab initio and DFT calculations for forward reaction 1 result in negative values of −1.5 and −3.0 kcal mol^{-1} at CBS-Q//MP2-(full)/6-31g(d) and CBS-Q//B3LYP/6-31g(d,p) levels, respectively, and positive barriers at G3MP2 level, 6.3 and 3.6 kcal mol^{-1} with MP2(full)/6-31g(d) and B3LYP/6-31g(d,p) geometries.

The Arrhenius preexponential factor for reaction 1 ($A_{\infty,1}$) is calculated via canonical TST with DFT determined structure parameters. The high-pressure limit rate constants, fit by a three-parameter (A, n, E_a) modified Arrhenius equation over a temperature range of 230 to 1500 K, are $2.47 \times 10^7 T^{1.7080}\exp(-808.8\ \text{cal}/RT)$ (s^{-1}) and $2.87 \times 10^{13} T^{0.14885}\exp(-19534\ \text{cal}/RT)$ $cm^3\ mol^{-1}\ s^{-1}$ for forward and reverse reaction 1, respectively, based on a G3 calculated barrier (0.86 kcal mol^{-1}). If we use these $k_{\infty,1}$ and $k_{\infty,-1}$ values, the resulting QRRK rate constant for C_6H_6 + OH → **C•HDOH** is underestimated by a factor of 0.13 compared to experimental data. To match the experimental data, we need to lower this G3 calculated barrier by 1.2 kcal mol^{-1} ($\Delta H°_{f,\ 298}$ of **TS1** is adjusted down by1.2 kcal mol^{-1}). $k_{\infty,1}$ and $k_{\infty,-1}$ are then $2.47 \times 10^7 T^{1.7080}\exp(391.2\ \text{cal}/RT)$ (s^{-1}) and $2.87 \times 10^{13} T^{0.14885}\exp(-18334\ \text{cal}/RT)$ $cm^3\ mol^{-1}\ s^{-1}$, respectively.

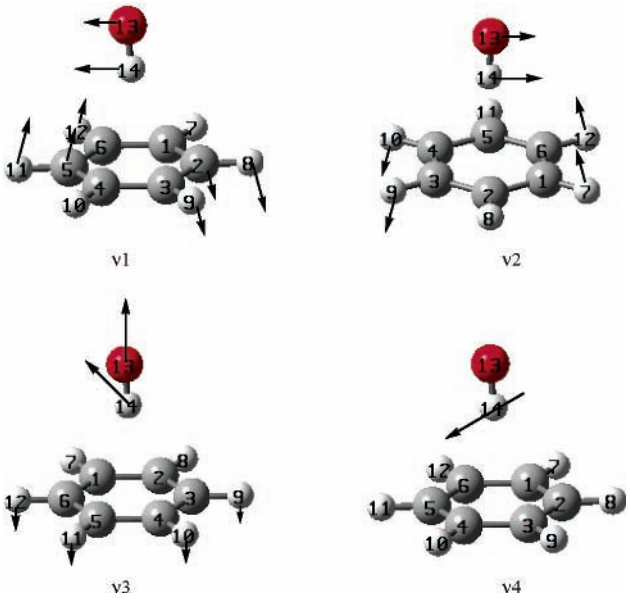

Figure 3. Corresponding normal mode vector of complex **PRII**.

Prereactive Complex(es) and IRC Analysis on Formation of Hydroxycyclohexadienyl Radical. One prereactive complex (**PRI**) is located at a geometry between the reactants and **TS1** at B3LYP/6-31g(d,p) level and has an energy 0.49 kcal mol^{-1} below reactants at a G3MP2//B3LYP/6-31g(d,p) calculation. The oxygen atom of OH is directed toward the carbon atom on the ring with a C−O bond distance of 2.5 Å. It has one very small imaginary vibration frequency ($17i$ cm^{-1}) corresponding to the O atom migration across the C−C═C in the ring. The vibration frequency ν_4 (134 cm^{-1}) corresponds to the reaction coordinate for the formation of complex (PRI) from reactants. We are unable to locate this **PRI** complex at MP2, HF and BH&HLYP level.

A second prereactive complex (**PRII**) is located at MP2(full)/6-31g(d), HF/6-31g(d,p), BH&HLYP/6-31g(d,p), and B3LYP/6-31g(d,p) levels. The OH radical in complex **PRII** is oriented perpendicular to the benzene ring plane, forming the weak interaction between H atom of OH radical and the π electron density of the benzene ring. A frequency calculation for complex **PRII** at MP2 level shows the lowest vibration frequency to be 57 cm^{-1} (29 and 24 cm^{-1} at HF and BH&HLYP, respectively); this frequency corresponds to the OH radical migration across the ring (along C2−C5 axis). The MP2 vibration frequency ν_3 (116 cm^{-1}) corresponds to the reaction coordinate for the formation of complex **PRII** from reactant molecules. DFT calculations on complex **PRII** show two imaginary vibration frequencies ($121i$ and $86i$ cm^{-1}) corresponding to migration of the H atom on the OH radical across the ring; these are determined to be 142 and 163 cm^{-1} with MP2. The enthalpy difference between reactants and complex **PRII** is 2.15 and 2.64 kcal mol^{-1} at G3MP2//MP2 and G3 calculations, respectively. Vibration frequencies of the prereactive complexes are listed in Table 1. The corresponding normal mode vector of complex **PRII** is given in Figure 3.

The reaction 1 takes place in two steps: first via formation of the prereactive complex (reaction 1a) and then via formation of the **C•HDOH** adduct (reaction 1b).

$$\text{benzene} + \text{OH} \leftrightarrow \text{complex (\textbf{PRII})} \qquad (1a)$$

$$\text{complex (\textbf{PRII})} \xleftrightarrow{\text{TS1}} \textbf{C•HDOH} \qquad (1b)$$

TABLE 6: Input Parameters and High-Pressure Limit Rate Constants (k_∞) for QRRK Calculation Benzene+ OH → Products[a]

reaction no.	reaction	A (s^{-1} or cm^3 mol^{-1} s^{-1})	n	α	E_a (kcal mol^{-1})	fnt.
1a	benzene + OH → **PRII**	1.56×10^8	3.4906	0.016 41	0.0	*b*
−1a	**PRII** → benzene + OH	6.30×10^6	4.4530	0.021891	2.51	*c*
1b	**PRII** → **C•HDOH** (via **TS1**)	1.02×10^{12}	0.085 14		2.56	*d*
−1b	**C•HDOH** → **PRII** (via **TS1**)	2.87×10^{13}	0.148 85		18.33	*e*
3	**C•HDOH** → phenol + H (via **TS3**)	3.06×10^6	2.159 83		20.74	*f*
4	**C•HDOH** → **I** (via **TS4**)	2.92×10^{12}	0.327 83		37.03	*e*
−4	**I** → **C•HDOH**	1.09×10^{12}	0.466 68		18.10	*c*
5	**I** → **II** (via **TS5**)	3.78×10^{11}	0.784 24		14.56	*e*
−5	**II** → **I**	1.36×10^{13}	−0.26403		9.10	*c*
6	**II** → **III** (via **TS6**)	2.17×10^{12}	0.300 07		19.41	*f*
−6	**III** → **II**	1.53×10^{11}	1.048 71		41.14	*c*
7	**II** → **PI** + H (via **TS7**)	7.51×10^7	1.4714		26.62	*f*
8	**II** → **PII** + H (via **TS8**)	4.03×10^{-5}	5.033 49		24.41	*f*
9	**III** → **PIII** + H (via **TS9**)	2.24×10^{-7}	5.984 62		35.76	*f*

[a] Geometric mean frequency. **PRII**: 416.1 (12.871), 1296.7 (15.813), 3302.3 cm^{-1} (7.317). C•HDOH: 521.2 (12.939), 1151.5 (14.538), 3165.2 cm^{-1} (8.023). **I**: 554.9 (14.536), 1353.9 (15.072), 3680.3 cm^{-1} (6.392). **II**: 503.9 (15.089), 1349.5 (15.999), 3999.8 cm^{-1} (4.913). **III**: 450.7 (12.049), 1226.4 (16.661), 3252.3 cm^{-1} (6.789). Lennard-Jones parameters: $\sigma = 5.5471$ Å, $\epsilon/k = 584.86$ K.[73] [b] Variational transition state theory with center-of- mass reaction coordinate approximation. Fit with the four-parameter modified Arrhenius equation $k = AT^n \exp(-\alpha T) \exp(-E_a/RT)$. [c] $\langle MR \rangle$. [d] Fit with the three-parameter modified Arrhenius equation $k = AT^n \exp(-E_a/RT)$; E_a reduced by 1.2 kcal mol^{-1}. [e] Fit with the three-parameter modified Arrhenius equation. [f] Fit with the three parameter modified Arrhenius equation; H tunneling effect has been included.

The high-pressure limit rate constant (k_∞) for forward reaction 1a is calculated employing a center-of-mass reaction coordinate in an *EJ*-resolved variational transition state theory evaluation as implemented in VARIFLEX.[46] The Monte Carlo integration is used for energy and total angular momentum (J) resolved calculation. A single binding energy (D_0) of 923.31 cm^{-1} is used. The potential energy surface calculated at G3//B3LYP/6-311++g(d,p) level of theory is obtained from that reported by Tokmakov et al.[16] The Varshni potential[47] is employed to represent the potential energy along the reaction coordinate.

$$V = D_e\{1 - (R_0/R)\exp[-\beta(R^2 - R_0^2)]\}^2 - D_e$$

where D_e is the dissociation energy excluding zero-point vibrational energy. R is the reaction coordinate, i.e., the distance between the two bonding atoms, and R_0 is the equilibrium value of R. Kinetic parameters for the reverse reaction (−1a) are calculated from thermodynamics and microscopic reversibility (MR) principles. The high-pressure limit rate constants ($k_{\infty,1a}$ and $k_{\infty,-1a}$) are listed in Table 6.

The Arrhenius preexponential factor, $A_{\infty,1b}$, is calculated via canonical TST along with MP2-determined entropies. The high-pressure rate for reaction 1b of **PRII** → **TS1** is calculated as $1.02 \times 10^{12}T^{0.08514}\exp(-3762 \text{ cal}/RT)$ (s^{-1}). To fit the QRRK rate (vs temperature) on C_6H_6 + OH → **C•HDOH** with experimental data, we needed to lower the E_a of reaction 1b, **PRII** → **TS1**, by 1.2 kcal mol^{-1}. With this adjustment, the high-pressure limit rate constant, $k_{\infty,1b}$, fit by a three-parameter (A, n, E_a) modified Arrhenius equation over the temperature range 230−1500 K, is $1.02 \times 10^{12}T^{0.08514}\exp(-2562 \text{ cal}/RT)$ (s^{-1}).

5b. C•HDOH ↔ Phenol + H Elimination Reaction (Reaction 3a). Phenol plus H atom is the most important product formation channel in the OH + benzene addition reaction system. The calculated energy barriers from **C•HDOH** are 26.3 kcal mol^{-1} at G3 and ∼27 kcal mol^{-1} at G3MP2 with B3LYP and MP2 geometries. The calculated barrier for reverse reaction (−3a), 7.3 kcal mol^{-1} by G3 method, is in agreement with the experimental data reviewed by Baulch et al.[44] (7.93 kcal mol^{-1}) and He et al.[48] (7.91 kcal mol^{-1}) while the G3MP2 calculated barriers for reaction (−3a) are higher by 4 and 6 kcal mol^{-1} with B3LYP and MP2 geometries, respectively. The CBS-Q method consistently underestimates energy barriers by ∼13 kcal $2mol^{-1}$ relative to than G3 for forward reaction 3a and by ∼9 kcal mol^{-1} for reverse reaction (−3a).

$$\mathbf{C^{\bullet}HDOH} \xleftrightarrow{\text{TS3}} \text{phenol} + \text{H} \qquad (3a)$$

Tunneling is incorporated into the high-pressure limit rate constants using the asymmetric Eckart calculation.[40−43] The tunneling factors (Γs) range from 54.2 to 1.2 between 300 and 2000 K. The high-pressure limit rate constant fit by a three-parameter modified Arrhenius equation over a temperature range of 300−2000 K is $3.06 \times 10^6T^{2.1598}\exp(-20740 \text{ cal}/RT)$ cm^3 mol^{-1} s^{-1} for forward reaction 3a. We have lowered the G3 calculated barrier on reaction 3a by 1.2 kcal mol^{-1} for consistency with the downward adjustment of the barrier on reaction 1b by 1.2 kcal mol^{-1}. This adjustment is based on assuming the same systematic errors apply for reactions 1b and 3a, which have similar TS structures involving radical addition to aromatic ring or resonance structures. Figure 4 shows a plot of G3 vs G3MP2//B3LYP addition barriers for the series of reactions below. The fit is quite linear, with a correlation coefficient R^2 of 0.998.

$$\text{C=CC}^{\bullet} + \text{O}_2 \rightarrow \text{C=CCOO}^{\bullet}$$

$$\text{C}_2^{\bullet}\text{C=C} + \text{O}_2 \rightarrow \text{C}_2\text{DCOO}^{\bullet}$$

$$\text{OH} + \text{benzene} \rightarrow \mathbf{C^{\bullet}HDOH}$$

$$\text{H} + \text{benzene} \rightarrow \text{C}^{\bullet}\text{HD}$$

$$\text{phenol} + \text{H} \rightarrow \mathbf{C^{\bullet}HDOH}$$

(addition to hydroxyl−carbon site)

Tokmakov and Lin[16] also lower their calculated G2 M(rcc,-MP2) and G3//B3LYP/6-311++G(d,p)) barrier (by ∼3.9 and ∼2.7 kcal mol^{-1}, respectively), to reach agreement with experimental data of the C_6H_6 + OH reaction.

5c. Formation of Bicyclo[3.1.0]hexan-6-ol Radical (I). The cyclopentadiene products (cyclopenta-2,4-dienylidenemethan-1-ol (**PI**), cyclopenta-2,4-dienecarbaldehyde (**PII**), and cyclopenta-1,3-dienecarbaldehyde (**PIII**)) are from the subsequent reactions of radical **I**. This bicyclic radical results from an intramolecular addition reaction by a carbon radical to a Π bond in **C•HDOH** (via **TS4**). Formation of this new intra-ring bond (reaction 4) involves coupling the unpaired electron with one

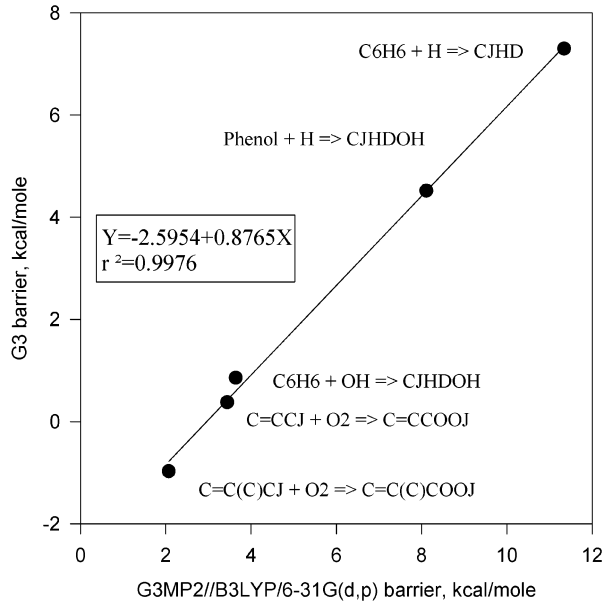

Figure 4. Addition barriers calculated at G3 vs G3MP2 for reactions of C═CC• + O_2 → C═CCOO•, C═C(C)C• + O_2 → C═C(C)COO•, C_6H_6+OH → **C•HDOH**, C_6H_6 + H → C•HD, phenol + H → **C•HDOH**. (J = radical site.)

of the two electrons of the Π bond being broken while the other Π electron is localized in the larger ring. The reaction has a relatively high barrier of 35−38 kcal mol^{-1}.

5d. Formation of Cyclopentadienes (Reactions 5−9). The cleavage of one exocyclic cyclopropane bond (via **TS5**) in the intermediate **I** (reaction 5) is endothermic (5.5 kcal mol^{-1}) with a 12−14 kcal mol^{-1} calculated barrier. The reaction results in intermediate **II** (cyclopenta-2,4-dienylmethan-1-ol radical)**,** which can react forward through three channels, or it can react back to the bicyclic radical with a low barrier. Two of the forward reaction paths involve β-scission (H atom elimination) reactions and the third path involves a combined H atom and double-bond shift. The two H atom elimination channels form either a cyclopenta-2,4-dienylidenemethan-1-ol with the hydroxy group on the methylene carbon **PI** or an aldehyde **PII**. The third reaction of radical **II** is a 1,2 H shift in concert with a corresponding diene shift through a lower barrier **TS6**. It forms a resonance stabilized intermediate **III** (cyclopentylidenemethan-1-ol) (reaction 6), where the diene in the ring is conjugated with the radical on the hydroxymethyl group, and conjugation extends through the radical site to the oxygen. The intermediate radical **III** will β-scission the hydroxyl hydrogen resulting in aldehyde **PIII** + H (reaction 9), where the diene is conjugated the carbonyl group.

The H atom eliminations (reactions 7 and 8) from the cyclopenta-2,4-dienylmethan-1-ol radical **II** to form **PI** (cyclopenta-2,4-dienylidenemethan-1-ol) + H (via **TS7**) and **PII (**cyclopenta-2,4-dienecarbaldehyde) + H (via **TS8**) are endothermic (26 and 24 kcal mol^{-1}) with respective barriers of 28 and 36 kcal mol^{-1}. The three-member ring ipso-carbon H-shift of **II** to the resonance stabilized radical **III** (reaction 6) has barrier of 20 kcal mol^{-1} which is lower than the barriers for H-elimination reactions 7 and 8. Intermediate **III** will β-scission the hydroxy hydrogen to form the cyclopenta-1,3-dienecarbaldehyde + H (via **TS9**) with a relatively high barrier of 48−52 kcal mol^{-1}, ΔH_{rxn} is 36 kcal mol^{-1}. The reverse reaction back to the bicyclo[3.1.0]hexan-6-ol radical **I** has the lowest overall barrier at ca. 7−13 kcal mol^{-1}.

These cyclopentadiene channels do not show high importance to forward reaction paths in this OH + benzene reaction system. This is due to the relatively tight transition states, loss of internal rotors, loss of ring bending modes, and the higher barriers relative to H + phenol or reverse reaction to OH + benzene. The reaction paths from association and addition reactions of smaller molecules and radicals that form and react through the resonance stabilized cyclopentadienes are, however, likely to be important in formation of benzene and phenol.

5e. OH Radical Abstraction H Atom (Reaction 2).

$$\text{benzene} + \text{OH} \overset{\text{TS2}}{\longleftrightarrow} \text{phenyl} + \text{H}_2\text{O} \qquad (2)$$

The G3 calculated barrier of 5.97 kcal mol^{-1} for OH abstraction reaction 2 is slightly higher than the experimental activation energies reported by Lin et al.[45] of 5.09 kcal mol^{-1}, Knispel et al.[5] of 3.28 kcal mol^{-1}, Tully et al.[2] of 4.49 kcal mol^{-1}, and Perry et al.[1]of 4.0 kcal mol^{-1}. The CBS-Q method again underestimates energy barriers relative to values calculated at G3MP2 by ∼5 kcal mol^{-1} and ∼3 kcal mol^{-1} for forward and reverse reaction 2. Both CBS-Q and G3MP2 with DFT geometry have lower barriers than with MP2 geometry by ∼6 and ∼1.5 kcal mol^{-1} for the respective forward and reverse reaction 2.

The rate constant includes H tunneling, using the enthalpy calculated at G3 ($\Delta H°_{f,\,298}$ of **TS2** is adjusted down by 1.2 kcal mol^{-1} for agreement with the experimental data and consistency with the downward adjustment on the G3 barrier on reaction 1b by 1.2 kcal mol^{-1}). Entropy and heat capacity values from vibrations and structure at B3LYP/6-31g(d,p) level of theory along with the hindered rotors contributions from internal barrier calculated at molecular mechanics force field (MMFF). We note that the G2M(rcc,MP2) and G3//B3LYP/6-311++G(d,p) calculated barriers, reported by Tokmakov and Lin,[16] are lowered by ∼2.0 and ∼0.7 kcal mol^{-1}, respectively. The rate constant in the form of three parameter modified Arrhenius equation is $1.20T^{4.10}$ exp(301cal/RT) cm^3 mol^{-1} s^{-1} for forward reaction 2.

Kinetic Analysis of Benzene + OH Reaction System. Data on the high-pressure rate constants, Lennard-Jones parameters, and vibration frequencies for the intermediates in the chemical activation calculations on benzene + OH reaction system are listed in Table 6. These parameters are used as input to the calculations using quantum RRK analysis for $k(E)$ and master equation for falloff in order to estimate rate constants to the varied products vs temperature (230−1500 K) and pressure ($0.5-10^5$ Torr). These QRRK calculations assume steady state for the energized intermediates. A detailed mechanism is used to study the overall reaction process vs time.

The QRRK/Master Equation calculated rate constants for forward reaction as a function of pressure at 298 K are illustrated in Figure 5, and rate constants as a function of temperature at 100 Torr are presented in Figure 6. Rate constants for OH + benzene **with the prereactive complex PRII**, are shown by filled symbols where reaction 1 takes place in two steps, 1a and 1b (system **A**). Rate constants determined **neglecting PRII** (system **B**) are shown as open symbols. Rate constants calculated with Ar bath gas are shown as solid lines and dashed lines are used to represent He bath gas.

For reaction system **A** which incorporates the prereactive adduct **PRII,** the energized **PRII*** complex primarily undergoes dissociation back to reactants. This is a result of the low barrier (3 kcal mol^{-1} well) and high preexponential factor for **PRII** dissociation to reactants. The unimolecular reaction from the **C•HDOH** adduct back to reactants also dominates all forward reaction paths of this adduct. The contribution of **PRII** to the overall kinetics is small and considered to be negligible; the

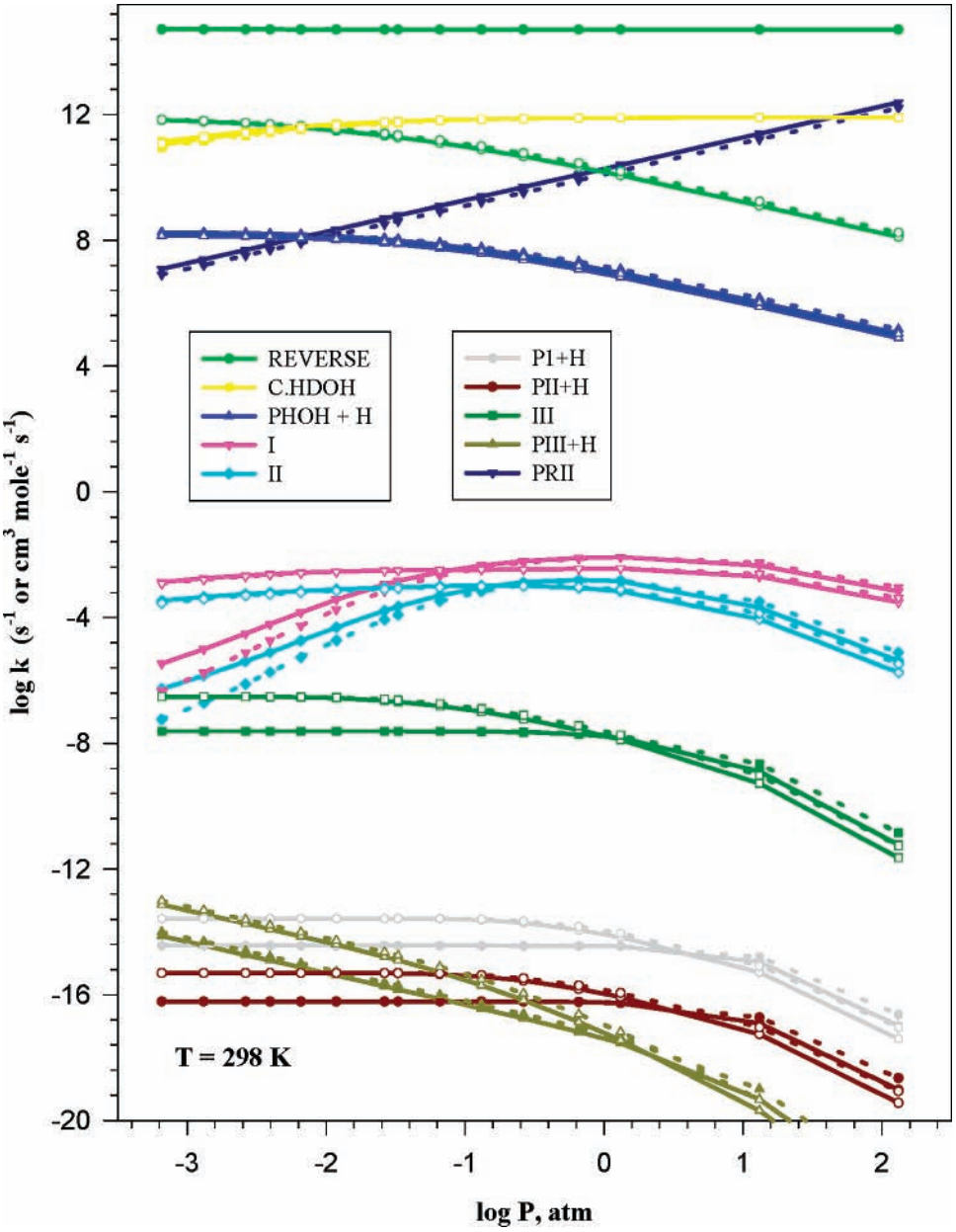

Figure 5. QRRK rates for OH + benzene as a function of temperature at pressure = 100 Torr. Rate constants for OH + benzene **with the prereactive complex PRII**, are shown by filled symbols where reaction 1 takes place in two steps, 1a and 1b (system **A**). Rate constants determined **neglecting PRII** (system **B**) are shown as open symbols. Rate constants calculated with Ar bath gas are shown as solid lines and dashed lines are used to represent He bath gas.

dissociation back to reactants is three or more orders of magnitude faster than stabilization to **PRII** over the entire temperature and pressure range.

In system **B** where the prereactive complex **PRII is neglected**, the energized **C•HDOH*** and stabilized **C•HDOH**° complexes primarily undergo dissociation back to reactants above 400 K; the stabilization to **C•HDOH** adduct dominates below 400 K. The two systems (**A** and **B**) predict almost the same $k(E)$ for formation of the **C•HDOH** adduct (deviation less than 10% below 800 K). The hydrogen atom elimination from the **C•HDOH** adduct to form phenol plus H becomes an important product channel with increasing temperature. It is faster than formation of products out of the varied cyclopentadiene intermediate adduct channels by at least 3 orders of magnitude below temperatures of 800 K. System A predicts a higher rate than system B for this phenol formation channel but predicts a lower rate by 1−2 orders of magnitude for cyclopentadiene product formation channels below 3 atm. Rates of isomerizations to cyclopentadiene intermediates are slightly higher in system A below 298 K and above 75 Torr, and become lower than values predict in system B with increasing temperature and decreasing pressure. Forward reaction through the cyclopentadiene intermediates do not appear to be important due to higher barriers.

Figure 7 illustrates high-pressure limit rates constants calculated in this study (application of canonical TST,[49] $S°_{298}$ and $C_p(T)$s from statistical mechanical analysis on all nontorsion frequencies, plus translations, external rotations, with partition functions for each hindered rotor, and electronic contributions). It also shows rate constants from the ChemRate[37] program which uses RRKM calculated values (internal rotor potentials assumed symmetric). The enthalpies of formation, moments of inertia and vibration frequencies required in ChemRate calculations use $\Delta H_f°_{298}$ determined from isodesmic reaction analysis (listed in Table 5) and B3LYP-determined molecular parameters (listed in Table 1). The rate constants of reactions 1 and 3a calculated

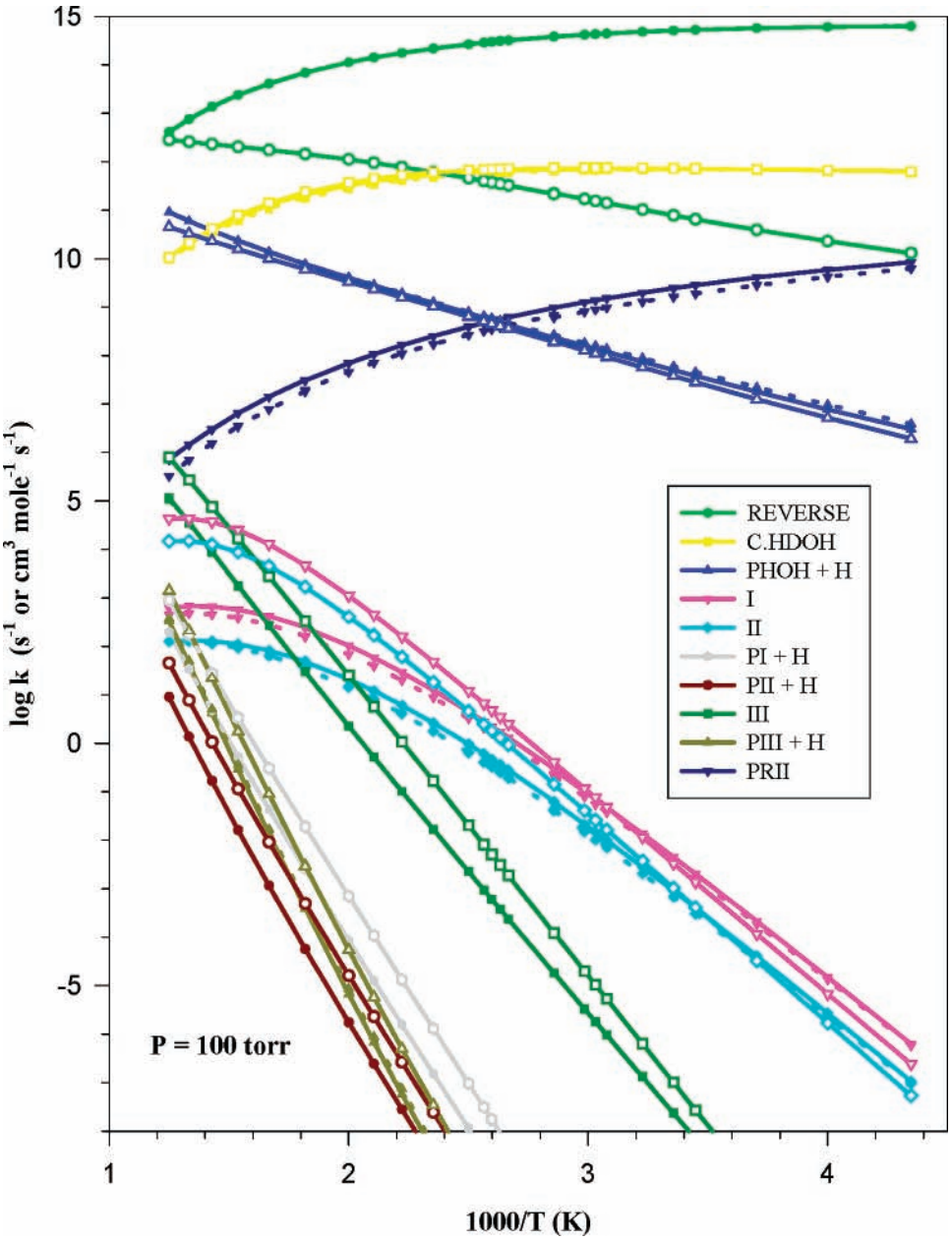

Figure 6. QRRK rates for OH + benzene as a function of pressure at 298 K.

from our QRRK analysis and from ChemRate RRKM theory are shown in Figure 7 (insert). Our QRRK rate constants are in good agreement with RRKM data at temperatures below 800 K (at $P = 100$ Torr).

Comparison of Kinetics and Model to Experimental Data. An elementary reaction mechanism (model) that includes the kinetic results of the chemical activation and the thermal dissociation analysis, as well as abstraction and other reactions of the intermediates, is used to model the system and to compare the calculated and experimental data. The mechanism also includes reactions that are specific to a given experiment, such as wall loss, or diffusion out of an optical path. The reaction mechanism, which is based on the OH + benzene reaction system A with prereactive complex **PRII,** is listed in Table 7 for a pressure of 100 Torr. It consists of 48 species and 97 reactions. The thermochemical parameters are listed in Table 4. The NASA format is given in the Supporting Information.

The CHEMKIN integrator code is utilized to calculate first-order OH radical decay rate (k') vs reaction time for 26 temperatures (230−1500 K), 9 pressures (0.5 Torr − 200 Torr), initial concentration of $[OH]_0 = 5 \times 10^{11}$ molecules cm^{-3}, and $[C_6H_6]_0/[OH]_0 = 80-500$. The bimolecular rate constant (k) for the overall reaction OH + benzene → products is computed from the slope of a linear least-squares fit of the k' vs benzene concentration. The plots of first-order OH radical decay rate (k') vs time (∼ 0.02 and ∼ 3 ms) and the k' vs benzene concentration are available in the Supporting Information.

We construct four elementary reaction mechanisms, one for each of four temperature regimes, to reduce the error between the fitted modified Arrhenius equation rate constants vs the specific QRRK calculated $k(T)$ values. The four temperature regimes used in the CHEMKIN integrator are as follows: (i) low (230−335 K); (ii) intermediate (335−550 K); (iii) high intermediate (550−1000 K); (iv) high (1000−1500 K). The comparison of our calculated rate constant and the literature rates are shown in Figure 8 (k vs pressure) and in Figure 9 (k vs temperature). The QRRK-calculated forward rate of addition

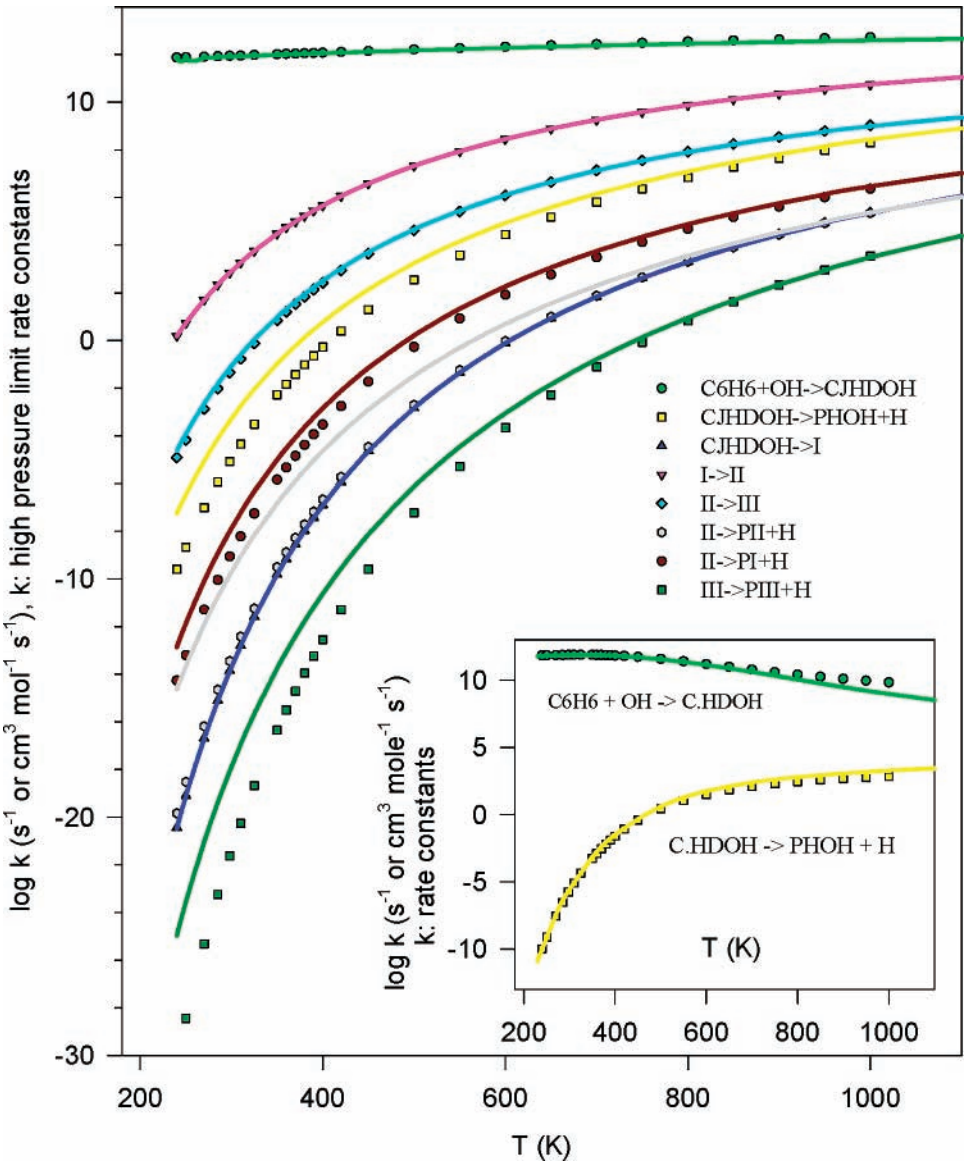

Figure 7. Comparison of high-pressure limit rates constants calculated from our analysis method and ChemRate program calculated values. Lines: QRRK. Points: ChemRate. The enthalpies of formation, moments of inertia and vibration frequencies required in ChemRate program calculations are used $\Delta H_f^\circ{}_{298}$ determined from isodesmic reaction analysis (listed in Table 5) and B3LYP-determined molecular parameters (listed in Table 1). Insert: comparison of pressure-dependent rate constants of reactions 1 and 3 between QRRK analysis and ChemRate RRKM theory. (J = radical site.)

pathway and rate for abstraction reaction studied in this work are also shown in Figure 9 (as solid and dotted lines, respectively).

Several experiments have reported rate constants (k) as a function of pressure at room temperature using flash (or laser) photolysis techniques with detection of the OH by resonance fluorescence. Our CHEMKIN calculated rate constants (*k*'s: lines with small symbols) shown in Figures 8 and 9 are in good agreement with experimental data (large symbols) under comparable conditions. Both experimental and calculated results demonstrate significant falloff behavior and negative temperature dependence. At room temperature the addition channel (C_6H_6 + OH → **C˙HDOH**) is ∼4 times faster than the abstraction reaction at 0.5 Torr and ∼27 times faster at 200 Torr.

Figure 9 illustrates a comparison of the rate constants (*k*) as a function of temperature (in different time windows) from CHEMKIN results at 100 Torr (Ar bath gas), with experimental data at the comparable conditions. The experimental results show the rate constant for OH + benzene → products increasing slightly as the temperature is raised from near 200 to 298 K. The calculated and the experimental data both show a dramatic decrease in rate constant with further increase in temperature. The forward rate constant resulting from the OH addition decreases until the abstraction becomes a competitive path for [OH] loss. The calculated data also illustrate that the experiments based on longer time measurements observe the decrease in the measured rate constant at lower temperature.

The one exception to the observed experimental decrease in OH decay rate with temperature increase above 298 K is reported by Wallington et al.[50] These experiments were performed at total pressures between 25 and 50 Torr, which are lower than other data ($P = \sim 100$ Torr). [OH] profiles from the experiments of both Tully et al.[2] and Perry et al.[1] exhibit nonexponential decays between ca. 320 and 400 K (325 K < *T* < 380 K, in Perry et al.'s work), and both studies indicate that the bimolecular rate constants decrease rapidly with increasing temperature. Above 400 K (380 K, in Perry et al.'s experiments), the decrease in rate constant turns over and it begins to increase with temperature. The temperature at which nonexponential OH decay occurs, for a given pressure, depends on the time

TABLE 7: Detailed Mechanism

reaction	A (s^{-1} or cm^3 mol^{-1} s^{-1})	n	E_a (cal mol^{-1})	T (K)	ref	reaction	A (s^{-1} or cm^3 mol^{-1} s^{-1})	n	E_a (cal mol^{-1})	T (K)	ref
$C_6H_6 + OH \leftrightharpoons$ **PRII**	3.18E+35	−9.8	2595	$230 \le T < 350$	*b*	duplicate reaction					
	1.53E+46	−13.4	4997	$350 \le T \le 550$	*b*	**C•HDOH** + H ⇔ CJHD + OH	1.43E−23	11.41	−829	230−1500	*b*
	3.09E+61	−18.2	10 664	$550 < T < 1000$	*b*	CHDOH ⇔ $C_6H_6 + H_2O$	1.49E+11	0	42 071	230−1500	*b*
	9.24E+302	−89.7	133 490	$1000 \le T \le 1500$	*b*	CHDOH ⇔ PHOH + H_2	1.82E+12	−0.36	52 315	230−1500	*b*
$C_6H_6 + OH \leftrightharpoons$ **C•HDOH**	7.73E+17	−2.1	1225	$230 \le T < 350$	*b*	CHDOH ⇔ CJHD + OH	2.73E+22	−2.3	73 517	230−1500	*b*
	8.63E+50	−13.1	9139	$350 \le T \le 550$	*b*	**C•HDOH** + OH ⇔ DIOH12CHD	8.69E+20	−2.62	1888	230−1500	*b*
	4.70E+88	−25	22 473	$550 < T < 1000$	*b*	**C•HDOH** + OH ⇔ PHOH + H_2O	5.14E−15	8.56	−2227	230−1500	*b*
	8.48E+258	−75.8	104 270	$1000 \le T \le 1500$	*b*	duplicate reaction					
$C_6H_6 + OH \leftrightharpoons$ PHOH + H	5.69E−03	4.9	3079	$230 \le T < 350$	*b*	DIOH12CHD ⇔ PHOH + H_2O	9.19E+10	0.07	42 028	230−1500	*b*
	1.63E+06	2	4905	$350 \le T \le 550$	*b*	**C•HDOH** + O ⇔ PHOH + OH	3.02E+13	0	0	230−1500	*b*
	7.34E+19	−2	11 433	$550 < T < 1000$	*b*	**C•HDOH** + OH_BZ_1 ⇔ DICHDOH	1.40E+12	0	0	230−1500	est.
	8.72E+178	−49.9	82 613	$1000 \le T \le 1500$	*b*	C_6H_6 + O ⇔ CJHDOJ	1.17E+59	−18.64	12 212	230−1500	*b*
$C_6H_6 + OH \leftrightharpoons$ **I**	1.40E+39	−10	22 972	$230 \le T < 350$	*b*	C_6H_6 + O ⇔ phenoxy + H	6.22E+13	−0.16	4408	230−1500	*b*
	2.27E+67	−19.4	29 619	$350 \le T \le 550$	*b*	CJHDOJ ⇔ phenoxy + H	4.68E+11	−0.26	7801	230−1500	*b*
	1.09E+100	−29.5	42 109	$550 < T < 1000$	*b*	C_6H_6 + H ⇔ C•HD	7.41E+47	−11.3	13 710	230−1500	*b*
	1.01E+284	−84.5	129 740	$1000 \le T \le 1500$	*b*	C_6H_6 + H ⇔ H_BZ_2	1.56E+67	−17.9	30 005	230−1500	*b*
$C_6H_6 + OH \leftrightharpoons$ **II**	1.46E+42	−11.2	23 939	$230 \le T < 350$	*b*	C_6H_6 + H ⇔ H_BZ_3	1.86E+70	−19.5	30 079	230−1500	*b*
	2.30E+70	−20.6	30 534	$350 \le T \le 550$	*b*	C_6H_6 + H ⇔ fulvene + H	4.80E+09	1.7	37 038	230−1500	*b*
	1.40E+93	−27.6	39 639	$550 < T < 1000$	*b*	C•HD ⇔ H_BZ_2	8.73E+53	−13.9	46 294	230−1500	*b*
	2.50E+277	−82.7	127 430	$1000 \le T \le 1500$	*b*	H_BZ_2 ⇔ H_BZ_3	2.64E+29	−5.1	28 192	230−1500	*b*
$C_6H_6 + OH \rightleftharpoons$ **PI** + H	3.27E+15	−1.9	34 469	$230 \le T < 350$	*b*	H_BZ_3 ⇔ fulvene + H	1.24E+22	−5.1	30 948	230−1500	*b*
	2.62E−09	6.5	29 737	$350 \le T \le 550$	*b*	CJHD + OH ⇔ $C_6H_6 + H_2O$	4.80E+08	2	0	230−1500	Dean et al.[51]
	7.21E+18	−1.8	41 997	$550 < T < 1000$	*b*	CJHD + H ⇔ $C_6H_6 + H_2$	1.80E+09	1.5	0	230−1500	Dean et al.[51]
	6.63E+180	−50.4	116 290	$1000 \le T \le 1500$	*b*	duplicate reaction					
$C_6H_6 + OH \rightleftharpoons$ **PII** + H	1.32E−04	4.3	31 179	$230 \le T < 350$	*b*	CJHD + H ⇔ CHD	2.65E+15	−0.8	579	230−1500	*b*
	2.92E−21	9.9	27 594	$350 \le T \le 550$	*b*	CJHD + H ⇔ $C_6H_6 + H_2$	1.63E−20	10.04	−3720	230−1500	*b*
	1.52E+05	2.2	39 171	$550 < T < 1000$	*b*	duplicate reaction					
	7.01E+166	−46.3	113 130	$1000 \le T \le 1500$	*b*	CHD ⇔ $C_6H_6 + H_2$	9.16E+09	0.4	51 750	230−1500	*b*
$C_6H_6 + OH \leftrightharpoons$ **III**	3.72E+05	2.1	25 138	$230 \le T < 350$	*b*	C_6H_6 + phenyl ⇔ CJHDPH	1.24E+76	−21.56	18 047	230−1500	*b*
	2.57E−02	4.5	23 459	$350 \le T \le 550$	*b*	C_6H_6 + phenyl ⇔ biphenyl + H	3.44E+05	2.09	8301	230−1500	*b*
	2.40E+74	−18.8	53 888	$550 < T < 1000$	*b*	CJHDPH ⇔ biphenyl + H	5.09E+30	−6.11	29 775	230−1500	*b*
	3.28E+284	−81.8	151 961	$1000 \le T \le 1500$	*b*	**C•HDOH** + HO_2 ⇔ CHDOHQ	8.22E+60	−15.9	12 032	230−1500	*b*
$C_6H_6 + OH \rightleftharpoons$ **PIII** + H	4.81E−46	18.4	22 662	$230 \le T < 350$	*b*	**C•HDOH** + HO_2 ⇔ CHDOHOJ + OH	1.21E+19	−1.7	8888	230−1500	*b*
	2.19E−61	23.8	20 054	$350 \le T \le 550$	*b*	CHDOHQ ⇔ CHDOHOJ + OH	9.43E+43	−9.3	51 452	230−1500	*b*
	3.57E+48	−10.1	61 259	$550 < T < 1000$	*b*	CHDOHOJ ⇔ ODCVVCJOH	2.15E+74	−20.1	20 092	230−1500	*b*
	1.53E+184	−51.2	117 940	$1000 \le T \le 1500$	*b*	CHDOHOJ ⇔ ODCVVCDO + H	5.86E+18	−1.4	29 441	230−1500	*b*
PRII ⇔ **C•HDOH**	8.65E+20	−3.3	16 674	$230 \le T < 350$	*b*	ODCVVCJOH ⇔ ODCVVCDO + H	1.55E+61	−16.5	50 899	230−1500	*b*
	1.27E+13	−0.7	14 576	$350 \le T \le 550$	*b*	**C•HDOH** + phenyl ⇔ CHDOHPH	1.11E+13	−0.02	11	230−1500	*b*
	1.34E+68	−16	48 965	$550 < T < 1000$	*b*	**C•HDOH** + phenyl ⇔ CJHDOHPH + H	1.46E−41	15.82	3165	230−1500	*b*
	3.09E+16	−1.98	6231	$1000 \le T \le 1500$	*b*	CHDOHPH ⇔ CJHDOHPH + H	1.27E+23	−3.24	85 928	230−1500	*b*
C•HDOH ⇔ PHOH + H	4.63E+22	−3.7	23 349	$230 \le T < 350$	*b*	CJHDOHPH ⇔ BIPHYLOH + H	6.39E+29	−6.22	16 849	230−1500	*b*
	4.79E+53	−14.1	30 648	$350 \le T \le 550$	*b*	phenyl + HO_2 = phenoxy + OH	3.00E+13	0	0	230−1500	*b*
	2.71E+26	−5.7	19 653	$550 < T < 1000$	*b*	phenyl + OH = PHOH	3.00E+13	0	0	230−1500	est.
	1.52E+42	−10.4	27 177	$1000 \le T \le 1500$	*b*	phenyl + H = C_6H_6	3.00E+13	0	0	230−1500	est.
C•HDOH ⇔ **I**	3.57E+42	−12.9	39 937	$230 \le T < 350$	*b*	PHOH + phenyl = C_6H_6+phenoxy	1.00E+11	0	6064	230−1500	est.
	1.67E+60	−18.8	44 086	$350 \le T \le 550$	*b*	PHOH + O_2 = phenoxy + HO_2	1.00E+13	0	37 900	230−1500	est.
	1.50E+24	−7.7	30 108	$550 < T < 1000$	*b*	PHOH + OH = phenoxy + H_2O	6.00E+12	0	0	230−1500	est.
	1.37E+48	−14.87	40 773	$1000 \le T \le 1500$	*b*	PHOH + O = phenoxy + OH	1.28E+13	0	2891	230−1500	Baulch et al.[52]
I ⇔ **II**	2.52E+44	−9.8	31 540	$230 \le T < 350$	*b*	PHOH + H = H_2+phenoxy	1.15E+14	0	12 390	230−1500	Baulch et al.[44]
	9.80E+63	−16.4	36 170	$350 \le T \le 550$	*b*	PHOH = H + phenoxy	1.09E+16	0	86 500	230−1500	est.
	2.89E+55	−13.9	31 889	$550 < T < 1000$	*b*	phenyl + O ⇔ phenoxy	4.12E+87	−26.8	13 185	230−1500	*b*
	1.35E+63	−16.2	35 485	$1000 \le T \le 1500$	*b*	phenyl + O ⇔ PH_4	1.69E+40	−14.9	2159	230−1500	*b*
II ⇒ **PI** + H	1.54E+32	−7.8	31 316	$230 \le T < 350$	*b*	phenyl + O ⇔ PH_5	5.31E−07	−0.8	−2832	230−1500	*b*
	3.67E+56	−15.9	37 130	$350 \le T \le 550$	*b*	phenyl + O ⇒ CJYPD + CO	4.48E+13	0	40	230−1500	*b*
	1.22E+43	−11.95	30 851	$550 < T < 1000$	*b*	phenoxy ⇔ PH_4	1.69E+22	−2.9	49 960	230−1500	*b*
	7.07E+53	−15.17	35 887	$1000 \le T \le 1500$	*b*	PH_4 ⇔ PH_5	1.81E+66	−16.5	51 891	230−1500	*b*

TABLE 7: Continued

reaction	A (s^{-1} or cm^3 mol^{-1} s^{-1})	n	E_a (cal mol^{-1})	T (K)	ref	reaction	A (s^{-1} or cm^3 mol^{-1} s^{-1})	n	E_a (cal mol^{-1})	T (K)	ref
II ⟹ **PII** + H	3.63E+21	−4.4	31 392	230 ≤ T < 350	*b*	PH_5 ⟹ CJYPD+CO	3.85E+44	−9.9	35 954	230−1500	*b*
	1.35E+46	−12.6	37 250	350 ≤ T ≤ 550	*b*	H + O_2 + M ↔ HO_2 + M	6.17E+17	−0.8	0	230−1500	Baulch et al.[52]
	4.13E+32	−8.62	30 959	550 < T < 1000	*b*	HO_2 + H ↔ H_2 + O_2	4.28E+13	0	1411	230−1500	Baulch et al.[44]
	4.90E+43	−11.94	36 082	1000 ≤ T ≤ 1500	*b*	HO_2 + H ↔ H_2O + O	3.01E+13	0	1721	230−1500	Baulch et al.[44]
II ↔ **III**	1.06E+41	−9.4	31 419	230 ≤ T < 350	*b*	HO_2 + H ↔ OH + OH	1.69E+14	0	874	230−1500	Baulch et al.[44]
	3.91E+65	−17.6	37 276	350 ≤ T ≤ 550	*b*	HO_2 + O ↔ OH + O_2	3.25E+13	0	0	230~1500	Baulch et al.[44]
	1.04E+52	−13.55	30 966	550 < T < 1000	*b*	HO_2 + OH ↔ O_2 + H_2O	2.89E+13	0	−497	230−1500	Baulch et al.[44]
	9.87E+62	−16.85	36 052	1000 ≤ T ≤ 1500	*b*	HO_2 + HO_2 ↔ O_2 + H_2O_2	1.87E+12	0	1540	230−1500	Baulch et al.[44]
III ⟹ **PIII** + H	1.69E−07	6	35 718	230 ≤ T < 350	*b*	H_2O_2 + H ↔ H_2 + HO_2	4.82E+13	0	7949	230−1500	Tsang et al.[58]
	2.00E−07	6	35 737	350 ≤ T ≤ 550	*b*	H_2O_2 + H ↔ H_2O + OH	2.41E+13	0	3974	230−1500	Tsang et al.[58]
	1.55E+21	−2.6	46 564	550 < T < 1000	*b*	H_2O_2 + O ↔ OH + HO_2	9.63E+06	2	3974	230−1500	Tsang et al.[58]
	2.64E+58	−13.7	64 350	1000 ≤ T ≤ 1500	*b*	H_2O_2 + OH ↔ HO_2 + H_2O	7.83E+12	0	1331	230−1500	Baulch et al.[44]
C_6H_6 + OH ⇔ phenyl + H_2O	1.20E+00	4.1	−301.1	230 ~ 1500	this study	H + O_2 ⇔ OH + O	1.99E+14	0	16 802	230−1500	Tsang et al.[58]
C_6H_6 + H ⇔ phenyl + H_2	5.07E+07	1.9	12 953	230−1500	Knyazev[36]	H_2 + OH = H_2O + H	1.02E+08	1.6	3300	230−1500	Baulch et al.[44]
C•HDOH + OH ↔ PHOH + H_2O	2.40E+08	2	0	230−1500	Dean et al.[51]	OH + OH ↔ O + H_2O	1.51E+09	1.1	99	230−1500	Baulch et al.[44]
duplicate reaction						OH + OH + M ↔ H_2O_2 + M	2.90E+17	−0.8	0	230−1500	Baulch et al.[44]
C•HDOH + H ↔ PHOH + H_2	9.00E+08	1.5	0	230−1500	Dean et al.[51]	O + H_2 ↔ OH + H	5.11E+04	2.7	6280	230−1500	Baulch et al.[44]
duplicate reaction						O + O + M ↔ O_2 + M	1.89E+13	0	−1788	230−1500	Tsang et al.[58]
C•HDOH + H ↔ CHDOH	7.63E+23	−3.6	2575	230−1500	*b*	H + O + M ↔ OH + M	4.71E+18	−1	0	230−1500	Tsang et al.[58]
C•HDOH + H ↔ C_6H_6 + H_2O	3.65E−06	5.73	−979	230−1500	*b*	H ⟹ wall	2.50E+02	0	0	230−1500	Peng et al.[72]
C•HDOH + H ↔ PHOH + H_2	1.43E−13	7.66	−1569	230−1500	*b*	OH ⟹ wall	8.80E+01	0	0	230−1500	Lin et al.[45]

[a] Rate constants in the form $AT^n \exp(-E_a/RT)$. Units: A factor, bimolecular, cm^3 mol^{-1} s^{-1}; A factor, unimolecular, s^{-1}; E_a, cal mol^{-1}. [b] From QRRK calculations. Pressure = 100 Torr. (J = radical site.)

resolution of the experimental technique. Explanation of this based on our mechanism analysis is described below.

Our QRRK and CHEMKIN calculations show very good agreement with the experimentally observed slow increase in rate at temperatures below 298 K. Our calculations also reproduce the data on exponential [OH] decay k' vs time (~20 ms) and linear k' vs [C_6H_6] concentrations between 230 K < T < 298 K (available in the Supporting Information). Above 325 K, the rate rapidly decreases as temperature increases, since the reverse reaction of **C•HDOH** becomes more important. This results in regeneration of OH radical and a decrease in [OH] decay with increase in temperature between 325 and 350 K. In this interval 325 K < T < 350 K, the [OH] decay k' is observed to be nonexponential vs time (~20 ms). OH loss does exhibit exponential decay at short reaction time, ≤5 ms, where the correlation coefficient on linear regressions of [OH] decays k' vs time are within 98%. The dash line with open square points in Figure 9 represents the CHEMKIN calculated rate constant (k) using the [OH] decay vs time (~5 ms); it shows good agreement with experimental values reported by Tully et al.[2] and Perry et al.[1] Our model predicted rate constant (k) at reaction time ~ 1 ms (dash line with triangle points in Figure 9) is in good agreement with the experimental rate constant from Lin et al.[45] In the CHEMKIN analysis, the bimolecular rates approaches that of the QRRK calculation values at time scales ~2×10^{-5} s.

When the reverse reaction of C_6H_6 + OH ↔ **C•HDOH** is omitted (forward reaction allowed, reverse not allowed) in the model, the CHEMKIN rate constants are identical to the sum of the QRRK forward rate via addition and the abstraction rate constants as shown in Figure 9 (dashed line with circle points). This provides support for our kinetic methods using ab initio and density functional results for most reaction processes (experimentally adjusted for several) with chemical activation and unimolecular dissociation with pressure falloff from our QRRK/master equation analysis and Chemkin with full reversibility for time dependence. The advantages of using Chemkin are at least 2-fold: (i) low temperatures can be treated readily; (ii) reactions outside the limited chemical activation system (where mass has to be conserved), e.g. abstraction or addition of a second oxygen (part II of this study) are allowed.

Figure 10 shows profiles of benzene, OH, H, O, **C•HDOH**, phenyl radical, H_2O, and phenol vs time (at 298 K as Figure 10a) and vs temperature (at time = 3 ms as Figure 10b). The data are from the OH + benzene reaction system with inclusion of the prereactive complex **PRII** at pressure = 100 Torr (Ar), initial concentration of OH radical = 5×10^{11} molecules cm^{-3}, and $[C_6H_6]_0/[OH]_0$ = 200. The concentration of **C•HDOH** increases slightly as the temperature increases, then decreases significantly above 335 K. The decrease in [**C•HDOH**] is due to (i) the increasing importance of reverse reaction C_6H_6 + OH ↔ **C•HDOH** with increasing temperature between 335 and 425 K), (ii) reaction to the phenol + H atom channel, and (iii) abstraction reaction (C_6H_6 + OH ↔ phenyl + H_2O) increasing in importance. Points i and iii result in reductions in **C•HDOH** and phenol formation. The oxygen atom source is the OH self-reaction, OH + OH ↔ O + H_2O, where the rate constant is obtained from the Baulch et al.[44] reported value of $1.5 \times 10^9 T^{1.14}$ exp(−100 cal/RT) cm^3 mol^{-1} s^{-1}.

The concentration of phenol increases with temperature up to 1000 K, above which it decreases. The formation of phenyl radical and H_2O also increase with temperature resulting from the increased importance of the abstraction reaction 2. We note that further reactions of phenyl radical should be included in

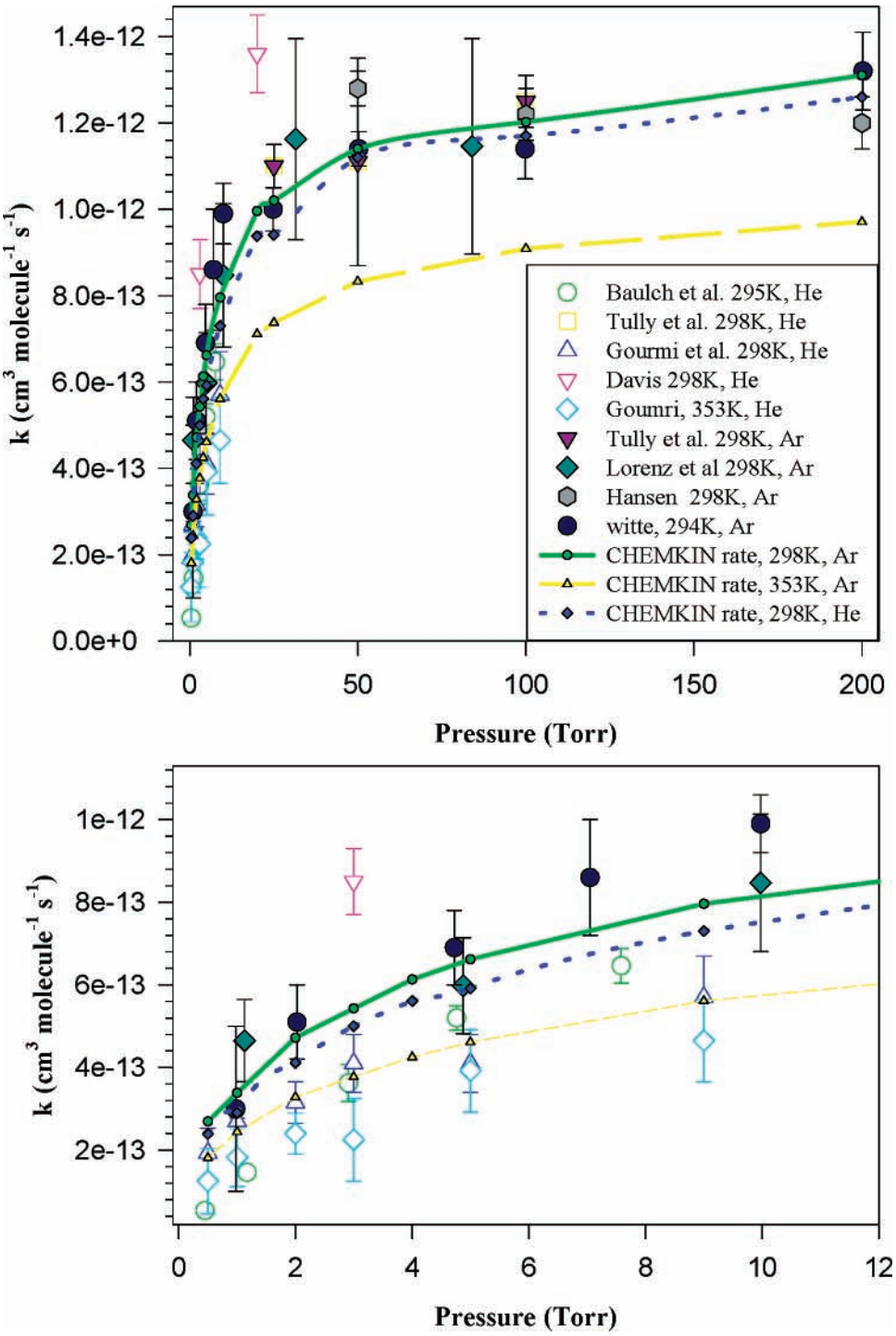

Figure 8. Comparison of our calculated rate constant and the literature rates (k vs pressure). Initial concentration of $[OH]_0 = 5 \times 10^{11}$ molecules cm^{-3}, and $[C_6H_6]_0/[OH]_0 = 80-500$.

the mechanism for a complete description in systems where O_2 is present. The loss of H atom is mainly via diffusion to the reactor walls, where a diffusion rate coefficient of 250 s^{-1} is used in the model. The H atom is produced along with the OH radical from ultraviolet photolysis of H_2O in refs 1, 2, 5, 34, and 40.

CHEMKIN sensitivity analysis on OH radical at pressure = 100 Torr and reaction time of 3 ms is shown in Figure 11. The OH addition to C_6H_6 to form **C•HDOH** is the most important reaction for [OH] decay. Its importance decreases with increasing temperature. Above 385 K, the abstraction reaction is more important than addition and its importance increases with increasing temperature. OH radical diffusion is an important loss channel between 300 and 600 K. The OH diffusion rate coefficient of 77 s^{-1} obtained from experimental data of Lin et al.[45] is used in the mechanism.

Bjergbakke et al.[8] reported phenol as the major ring-retaining product with a yield of about 24−25% in pulse radiolysis of $Ar/H_2O/C_6H_6$ mixtures at 1 atm and 298 K. CHEMKIN sensitivity analysis on phenol formation is shown in Figure 12 with five reactions showing high sensitivity to phenol formation at 298 K, 1 atm, initial concentration of $[OH]_0 = [H]_0 = 5.5 \times 10^{14}$ molecules cm^{-3} (H atom is from initiation reaction: $Ar^* + H_2O \rightarrow Ar + H + OH$, where we assume the H atom and

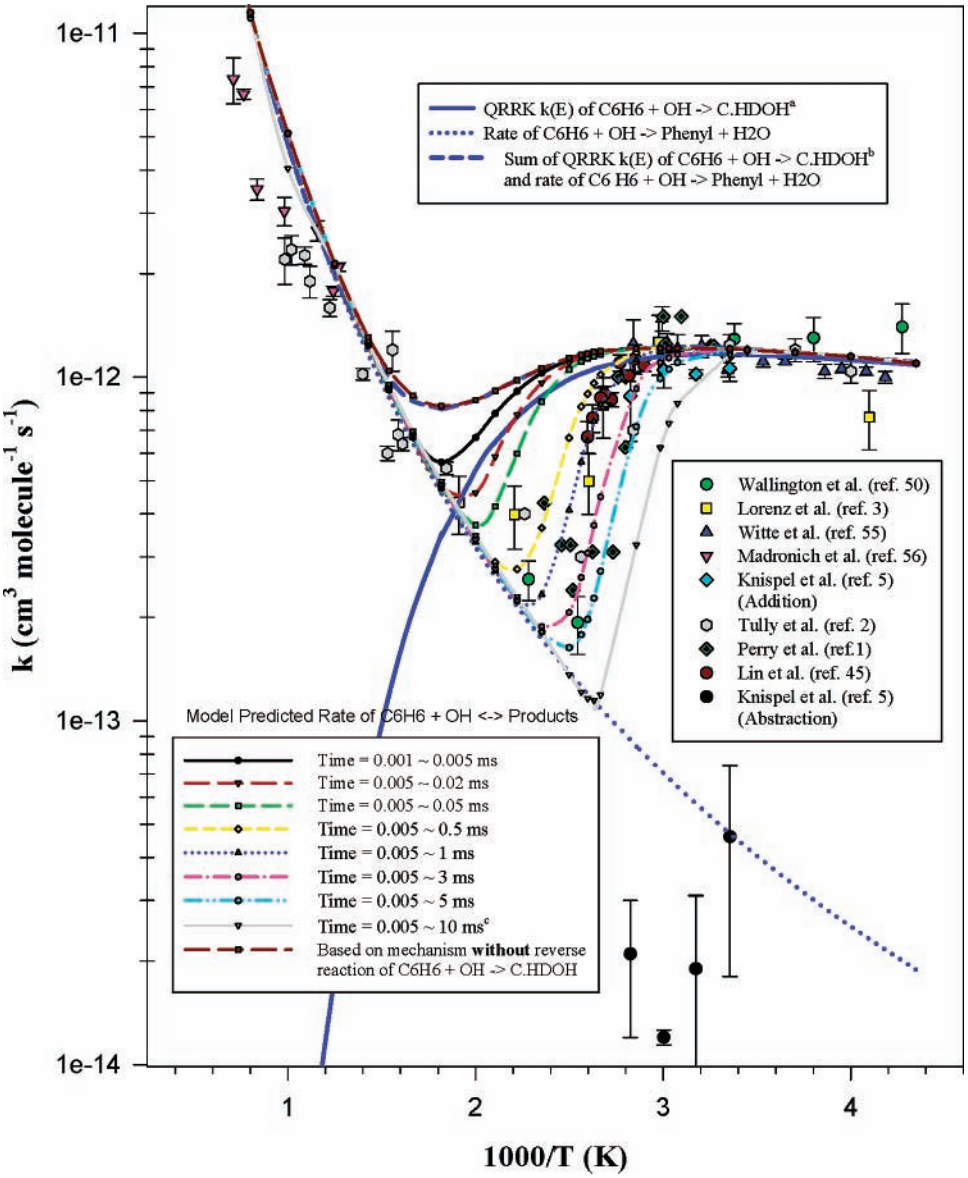

Figure 9. Comparison of our calculated rate and the experiment data (k vs temperature). Initial concentration of $[OH]_0 = 5 \times 10^{11}$ molecules cm^{-3}, and $[C_6H_6]_0/[OH]_0 = 80-500$ with Ar bath gas. (a) This only corresponds to experiment data at a very short time, ca. 10^{-5} s (where almost no reverse reaction from stabilized C•HDOH occur). (b) This shows the chemical activation reaction of C•HDOH (where no C•HDOH° dissociation to benzene + OH is allowed). (c) At longer time, more C•HDOH is formed and reacts back to benzene + OH, resulting in lower observed OH decay.

OH radical are produced in the same initiation concentration), and $[C_6H_6]_0/[OH]_0 = 180$.

(i) **C•HDOH** radical plus H atom (abstraction) forms phenol + H_2

$$\mathbf{C^{\bullet}HDOH} + H \leftrightarrow \text{phenol} + H_2 \quad (10)$$

(ii) **C•HDOH** radical−H radical combination reaction

$$\mathbf{C^{\bullet}HDOH + H \leftrightarrow CHDOH} \quad (11)$$

(iii) OH abstraction of H from **C•HDOH** forms phenol + H_2O

$$\mathbf{C^{\bullet}HDOH} + OH \leftrightarrow \text{phenol} + H_2O \quad (13)$$

(iv) H addition to benzene forms **C•HD** radical

$$C_6H_6 + H \leftrightarrow \mathbf{C^{\bullet}HD} \quad (12)$$

(v) OH addition to benzene forms **C•HDOH** radical (1)

The rates for reactions 10 and 13 are estimated as $2.4 \times 10^8 T^{2.0}$ and $9.0 \times 10^8 T^{1.5}$ cm^3 mol^{-1} s^{-1}, respectively, following the procedure from Dean and Bozzelli[51] for abstraction rate constants by H and OH radicals, and fit experimental data yield of 24% phenol. Analysis of rate using the reaction mechanism shows that a decrease in the preexponential factor (A) in reaction 10 by a factor of 2 results in a decrease of phenol formation by 56% (yield of phenol of 10%) at 298 K and 1 atm (reaction time = 0.3 s). The rate constant for reaction 11 is estimated as 1×10^{13} cm^3 mol^{-1} s^{-1}. High-pressure limit rate constant of reaction 12, $1.84 \times 10^{11} T^{0.91526} \exp(-5392.9 \text{ cal}/RT)$ cm^3 mol^{-1} s^{-1}, is calculated via canonical TST along with DFT-determined entropies and G3 calculated barrier. Reaction 10 contributes 98% of phenol formation. This is in disagreement with the pathway suggested by Bjergbakke et al.;[8] they suggest the reaction 3a **C•HDOH** ↔ phenol + H with rate constant of 1.7×10^{11} cm^3 mol^{-1} s^{-1} at 298 K is major channel for phenol formation. We note that our rate constants for reaction 3a are 1.2×10^7 cm^{3}mol^{-1} s^{-1} at 298 K and 1.9×10^{11} cm^3 mol^{-1} s^{-1} at 1000

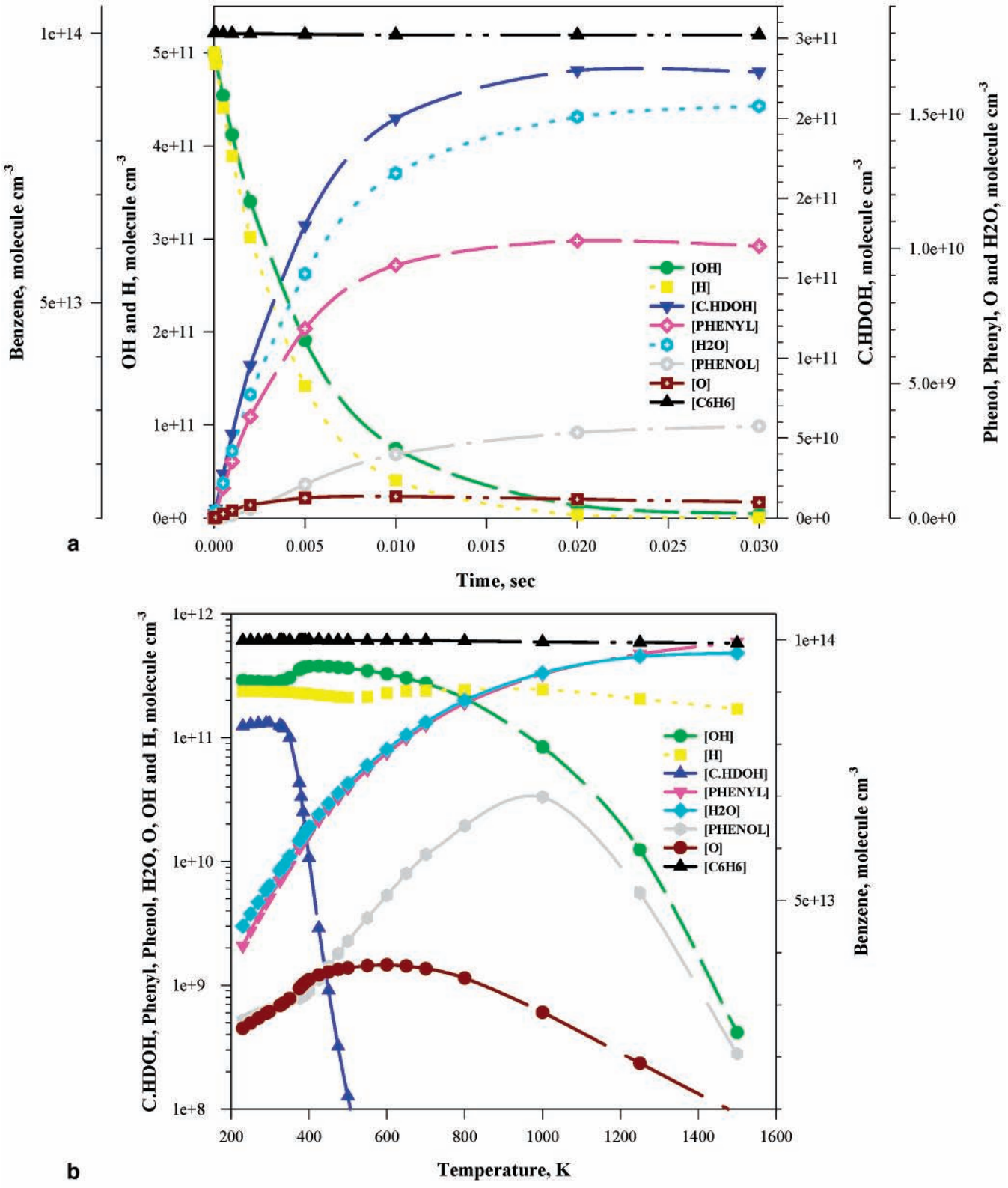

Figure 10. (a) The concentrations vs time based on the OH + benzene reaction system with inclusion of the prereactive complex **PRII** at 298 K, $[OH]_0 = 5 \times 10^{11}$ molecules cm^{-3}, $[C_6H_6]_0/[OH]_0 = 200$ with Ar bath gas. (b) The concentrations of benzene, OH, H, O, **C•HDOH**, phenyl radical, H_2O, and phenol vs temperature based on the OH + benzene reaction system with inclusion of the prereactive complex **PRII** at pressure = 100 Torr, $[OH]_0 = 5 \times 10^{11}$ molecules cm^{-3}, $[C_6H_6]_0/[OH]_0 = 200$, and reaction time of 3 ms with Ar bath gas.H atom is from initiation reaction: Ar* + $H_2O \rightarrow$ Ar + H + OH, (as per experiment description) where we assume the H atom and OH radical are produced in the same initiation concentration.

K, the latter of which is close to the value of 6.5×10^{10} cm^3 mol^{-1} s^{-1} reported by Baulch et al.[44] and He et al.[48] at 1000 K.

Summary

A thermochemical and chemical activation reaction analysis is presented on the important reaction system: benzene + OH.

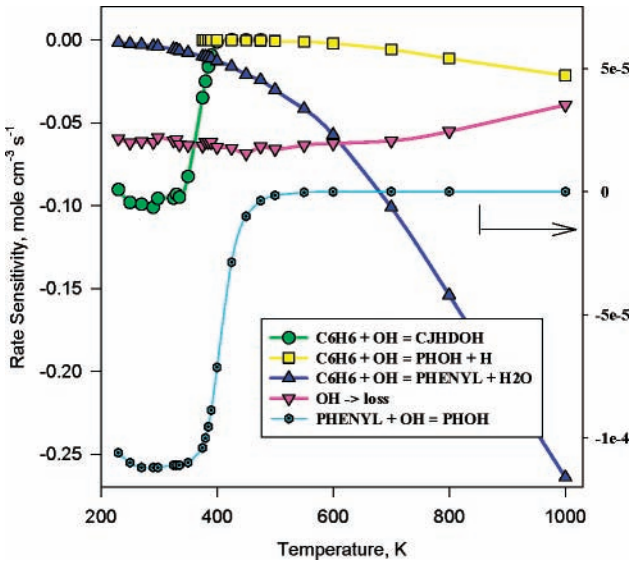

Figure 11. CHEMKIN sensitivity analysis on OH radical at pressure = 100 Torr, $[OH]_0 = 5 \times 10^{11}$ molecules cm^{-3}, $[C_6H_6]_0/[OH]_0 = 200$ and reaction time of 3 ms. (J = radical site.)

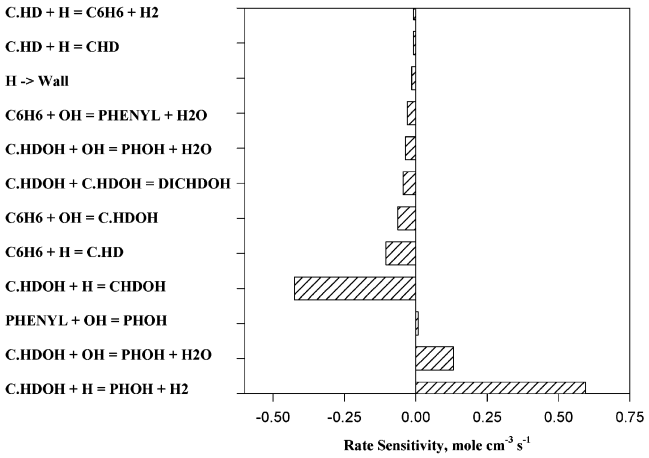

Figure 12. CHEMKIN sensitivity analysis on phenol formation at 298 K, 1 atm, initial concentration of $[OH]_0 = [H]_0 = 5.5 \times 10^{14}$ molecules cm^{-3} (H atom is from reaction Ar* + H_2O → Ar + H + OH), and $[C_6H_6]_0/[OH]_0 = 180$.

Thermodynamic proprieties, reaction paths and elementary reactions are presented with kinetic parameters evaluated vs temperature and pressure. An elementary reaction mechanism with microscopic reversibility has been developed to model OH radical reaction with benzene over the temperature range from 230 to 1500 K and to model the experimental bimolecular rate constant of benzene + OH → products. Comparison of our calculated constants with experimental data from varied temperature and pressure condition sets show very good agreement and illustrate that microscopic reversibility needs to be included in analysis of experimental data on this reaction.

Supporting Information Available: A table of the geometries of species used in this work figures showing plots of first-order OH radical decay, k' vs benzene concentration, and tables of THERMO data in NASA format and the mechanism listing and pressure dependent rate constants. This material is available free of charge via the Internet at http://pubs.acs.org.

References and Notes

(1) Perry, R. A.; Atkinson, R.; Pitts, J. N., Jr. *J. Phys. Chem.* **1977**, *81*, 296.
(2) Tully, F. P.; Ravishankara, A. R.; Thompson, R. L.; Nicovich, J. M.; Shah, R. C.; Kreutter, N. M.; Wine, P. H. *J. Phys. Chem.* **1981**, *85*, 2262.
(3) Lorenz, K.; Zellner, R. *Ber. Bunsen-Ges. Phys. Chem.* **1983**, *87*, 629.
(4) Wahner. A.; Zetzsch, C. *J. Phys. Chem.* **1983**, *87*, 4945.
(5) Knispel, R.; Koch, R.; Siese, M.; Zetzsch, C. *Ber. Bunsen-Ges. Phys. Chem.* **1990**, *94*, 1375.
(6) Goumri, A.; Pauwels, J. F.; Devolder, X. *Phys. Can. J. Chem.* **1991**, *69*, 1057.
(7) Venkat, C.; Brezinsky, K.; Glassman, I. *19th Combustion Symposium*, 1982; p 143.
(8) Bjergbakke, E.; Sillensen, A.; Pagsberg, P. *J. Phys. Chem.* **1996**, *100*, 5729.
(9) Berndt, T.; Boge, O.; Herrmann, H. *Chem. Phys. Lett.* **1999**, *314*, 435−42.
(10) Volkamer, R.; Klotz, B.; Barnes, I.; Imamura, T.; Wirtz, K.; Washida, N.; Becker, K. H.; Platt, U. *Phys. Chem. Chem. Phys.* **2002**, *4*, 1598.
(11) Alzueta, M. U.; Glarborg, P.; Dam-Johansen, K. *Int. J. Chem. Kinet.* **2000**, *32*, 498.
(12) Lay, T. H.; Bozzelli, J. W.; Seinfeld, J. H. *J. Phys. Chem.* **1996**, *100*, 6543.
(13) Cheney, B. V. *THEOCHEM* **1996**, *364*, 219.
(14) Berho, F.; Rayez, M.-Th.; Lesclaux, R. *J. Phys. Chem.* **1999**, *103*, 5501.
(15) Barckholtz, C.; Barckholtz, T. A.; Hadad, C. M. *J. Phys. Chem.* **2001**, *105*, 140.
(16) Tokmakov, I. V.; Lin, M. C. *J. Phys. Chem.* **2002**, *106*, 11309.
(17) Chen, C.; Lay, T. H.; Bozzelli, J. W. *J. Phys. Chem.* **2003**, *107*, 6451−6456.
(18) Frisch, M. J.; Trucks, G. W.; Schlegel, H. B.; Scuseria, G. E.; Robb, M. A.; Cheeseman, J. R.; Zakrzewski, V. G.; Montgomery, J. A., Jr.; Stratmann, R. E.; Burant, J. C.; Dapprich, S.; Millam, J. M.; Daniels, A. D.; Kudin, K. N.; Strain, M. C.; Farkas, O.; Tomasi, J.; Barone, V.; Cossi, M.; Cammi, R.; Mennucci, B.; Pomelli, C.; Adamo, C.; Clifford, S.; Ochterski, J.; Petersson, G. A.; Ayala, P. Y.; Cui, Q.; Morokuma, K.; Rega, N.; Salvador, P.; Dannenberg, J. J.; Malick, D. K.; Rabuck, A. D.; Raghavachari, K.; Foresman, J. B.; Cioslowski, J.; Ortiz, J. V.; Baboul, A. G.; Stefanov, B. B.; Liu, G.; Liashenko, A.; Piskorz, P.; Komaromi, I.; Gomperts, R.; Martin, R. L.; Fox, D. J.; Keith, T.; Al-Laham, M. A.; Peng, C. Y.; Nanayakkara, A.; Challacombc, M.; Gill, P. M. W.; Johnson, B.; Chen, W.; Wong, M. W.; Andres, J. L.; Gonzalcz, C.; Head-Gordon, M.; Replogle, E. S.; Pople, J. A. *Gaussian 98*, Revision A.11.4. Gaussian Inc.: Pittsburgh, PA, 2002.
(19) (a) Becke, A. D. *J. Chem. Phys.* **1993**, *98*, 5648. (b) Becke, A. D. *Phys. Rev. A* **1988**, *38*, 3098. (c) Lee, C.; Yang, W.; Parr, R. G. *Phys. Rev. B* **1988**, *37*, 785. (d) Stephens, P. J.; Devlin, F. J.; Chabalowski, C. F.; Frisch, M. J. *J. Phys. Chem.* **1994**, *98*, 11623.
(20) Ochterski, J. W.; Petersson, G. A.; Montgomery, J. A. *J. Chem. Phys.* **1996**, *104*, 2598.
(21) Montgomery, J. A.; Frisch, J. W.; Ochterski, J. W.; Petersson, G. A.; Raghavachari, K.; Zakrzewski, V. G. *J. Chem. Phys.* **1998**, *109*, 6505.
(22) Montgomery, J. A.; Frisch, J. W.; Ochterski, J. W.; Petersson, G. A. *J. Chem. Phys.* **1999**, *110*, 2822.
(23) Curtiss, L. A.; Redfern, P. C.; Raghavachari, K.; Rassolov, V.; Pople, J. A. *J. Chem. Phys.* **1999**, *110*, 4703.
(24) Curtiss, L. A.; Raghavachari, K.; Redfern, P. C.; Rassolov, V.; Pople, J. A. *J. Chem. Phys.* **1998**, *109*, 7764.
(25) Chen, C.; Bozzelli, J. W. *J. Phys. Chem.* **2000**, *104*, 9715.
(26) Lay, T. H.; Krasnoperov, L. N.; Venanzi, C. A.; Bozzelli, J. W. *J. Phys. Chem.* **1996**, *100*, 8240.
(27) McQuarrie, D. A. *Statistical mechanics*; Harper & Row: New York, 1976.
(28) Ritter, E. R. *Int. J. Chem. Kinet.* **1997**, *29*, 161.
(29) Ritter, E. R. *J. Chem. Inf. Comput. Sci.* **1991**, *31*, 400.
(30) Bozzelli, J. W.; Dean, A. M.; Chang, A. *Int. J. Chem. Kinet.* **1997**, *29*, 161.
(31) Chang, A. Y.; Bozzelli, J. W.; Dean, A. M. *Z. J. Phys. Chem.* **2000**, *104*, 1533.
(32) Sheng, C.; Bozzelli, J. W.; Dean, A. M.; Chang, A. Y. *J. Phys. Chem.* **2002**, *106*, 7276.
(33) Chen, C.-J.; Bozzelli, J. W. *J. Phys. Chem.* **1999**, *103*, 9731.
(34) Sun, H.; Bozzelli, J. W, *J. Phys. Chem.* **2004**, ASAP article.
(35) Troe, J. In *Combustion Chemistry*; Gardiner, W. C., Jr., Ed.; Springer-Verlag: NY, **1984.**
(36) Knyazev, V. D. *J. Phys. Chem.* **1996**, *100*, 5318.
(37) Mokrushin, V.; Bedanov, V.; Tsang, W.; Zachariah, M. R.; Knyazev, V. D. *ChemRate, Version 1.19*; National Institute of Standards and Technology: Gaithersburg, MD 20899, 2002.
(38) Kee, R. J.; Rupley, F. M.; Miller, J. A.; Coltrin, M. E.; Grcar, J. F.; Meeks, E.; Moffat, H. K.; Lutz, A. E.; Dixon-Lewis, G.; Smooke, M. D.; Warnatz, J.; Evans, G. H.; Larson, R. S.; Mitchell, R. E.; Petzold, L.

R.; Reynolds, W. C.; Caracotsios, M.; Stewart, W. E.; Glarborg, P.; Wang, C.; Adigun, O. CHEMKIN Collection, Release 3.6, Reaction Design, Inc., San Diego, CA 2001.

(39) Scott, A. P.; Radom, L. *J. Phys. Chem.* **1996**, *100*, 16502.

(40) Yamada, T.; Bozzelli, J. W. *J. Phys. Chem.* **1999**, *103*, 7646.

(41) Schwartz, M.; Marshall, P.; Berry, R. J.; Ehlers, C. J.; Petersson, G. A. *J. Phys. Chem.* **1998**, *102*, 10074.

(42) Louis, F.; Gonzalez, C. A.; Huie, R. E.; Kurylo, M. J. *J. Phys. Chem.* **2000**, *104*, 2931.

(43) Knyazev, V. D.; Bencsura, A.; Stoliarov, S. I.; Slagle, I. R. *J. Phys. Chem.* **1996**, *100*, 11346.

(44) Baulch, D. L.; Cobos, C. J.; Cox, R. A.; Esser, C.; Frank, P.; Just, Th.; Kerr, J. A.; Pilling, M. J.; Troe, J.; Walker, R. W.; Warnatz, J. *J. Phys. Chem. Ref. Data* **1992**, *21*, 411.

(45) Lin, S.-C.; Kuo, T.-C.; Lee, Y.-P. *J. Chem. Phys.* **1994**, *101*, 2098.

(46) Klippenstein, S. J.; Wagner, A. F.; Dunbar, R. C.; Wardlaw, D. M.; Robertson, S. H. VARIFLEX; VERSION 1.00 ed.; Argonne National Laboratory: Argonne, IL 60439, 1999.

(47) Varshni, Y. P. *Rev. Mod. Phys.* **1957**, *29*, 664.

(48) He, Y. Z.; Mallard, W. G.; Tsang, W. *J. Phys. Chem.* **1988**, *92*, 2196.

(49) Steinfeld, J. I.; Franciso, J. S.; Hase, W. L. *Chemical Kinetics and Dynamics*; Prentice Hall: Engelwood Cliffs, NJ, 1989.

(50) Wallington, T. J.; Neuman, D. M.; Kurylo, M. J. *Int. J. Chem. Kinet.* **1987**, *19*, 725.

(51) Dean, A. M.; Bozzelli, J. W. Analysis of Hydrogen Atom Abstraction Reactions. *Comb. Chem. Nitro.* **1997**, *1*, 12−15.

(52) Baulch, D. L.; Campbell, I. M.; Saunders, S. M. *J. Chem. Soc., Faraday Trans.* 2, **1988**, *84*, 377.

(53) Davis, D. D.; Bollinger, W.; Fischer, S. J. *J. Phys. Chem.* **1975**, *79*, 293.

(54) Hansen, D. A.; Atkinson, R.; Pitts, J. N. Jr. *J. Phys. Chem.* **1975**, *79*, 1763.

(55) Witte, F.; Urbanik, E.; Zetzsch, C. *J. Phys. Chem.* **1986**, *90*, 3251.

(56) Mardronich, S. Felder, W. *J. Phys. Chem.* **1985**, *89*, 3556.

(57) Baulch, D. L.; Cobos, C. J.; Cox, R. A.; Frank, P.; Hayman, G.; Just, Th.; Kerr, J. A.; Murrells, T.; Pilling, M. J.; Troe, J.; Walker, R. W.; Warnatz, J. *J. Phys. Chem. Ref. Data* **1994**, *23*, 847.

(58) Tsang, W.; Hampson, R. F. *J. Phys. Chem. Ref. Data* **1986**, *15*, 1087.

(59) Chase, M. W., Jr. *J. Phys. Chem. Ref. Data, Monogr. 9*, **1998**, 1.

(60) Pittam, D. A.; Pilcher, G. *J. Chem. Soc., Faraday Trans. 1* **1972**, *68*, 2224.

(61) Prosen, E. J.; Maron, F. W.; Rossini, F. D. *J. Res. NBS* **1951**, *46*, 106.

(62) Lacher, J. R.; Walden, C. H.; Lea, K. R.; Park, J. D. *J. Am. Chem. Soc.* **1950**, *72*, 331.

(63) Zhu, L.; Chen, C. J.; Bozzelli, J. W. *J. Phys. Chem.* **2000**, *104*, 9197.

(64) Cohen, N. *J. Phys. Chem. Ref. Data* **1996**, *25*, 1411.

(65) Wiberg, K. B.; Crocker, L. S.; Morgan, K. M. *J. Am. Chem. Soc.* **1991**, *113*, 3447.

(66) Snelson, A.; Skinner, H. A. *Trans. Faraday Soc.* **1961**, *57*, 2125.

(67) Connett, J. E. *J. Chem. Thermodyn.* **1975**, *7*, 1159.

(68) Knowlton, J. W.; Rossini, F. D. *J. Res. NBS* **1949**, *43*, 113.

(69) Allinger, N. L.; Dodziuk, H.; Rogers, D. W.; Naik, S. N. *Tetrahedron* **1982**, *38*, 1593.

(70) Roth, W. R.; Adamczak, O.; Breuckmann, R.; Lennartz, H.-W.; Boese, R. *Chem. Ber.* **1991**, *124*, 2499.

(71) Tsang, W Heats of Formation of Organic Free Radicals by Kinetic Methods In *Energetics of Organic Free Radicals*; Martinho Simoes, J. A., Greenberg, A., Liebman, J. F. Eds., Blackie Academic and Professional: London, 1996; pp 22−58.

(72) Peng, J.; Hu, X.; Marshall, P. *J. Phys. Chem.* **1999**, *103*, 5307.

(73) Hirschfelder, J. O.; Curtiss, C. F.; Bird, R. B. *Molecular Theory of Gases and Liquids*, 2nd ed.; Wiley: London, 1963.